

Accepted Manuscript

# *Journal of the Geological Society*

## The Red Sea rifting in central Egypt: constraints from the offshore Quseir

Moamen Ali, Alessandro Decarlis, Marco Ligi, Philip Ball, William Bosworth & Andrea Ceriani

DOI: <https://doi.org/10.1144/jgs2022-105>

To access the most recent version of this article, please click the DOI URL in the line above. When citing this article please include the above DOI.

Received 14 July 2022

Revised 7 November 2022

Accepted 13 November 2022

© 2022 The Author(s). Published by The Geological Society of London. All rights reserved. For permissions: <http://www.geolsoc.org.uk/permissions>. Publishing disclaimer: [www.geolsoc.org.uk/pub\\_ethics](http://www.geolsoc.org.uk/pub_ethics)

### **Manuscript version: Accepted Manuscript**

This is a PDF of an unedited manuscript that has been accepted for publication. The manuscript will undergo copyediting, typesetting and correction before it is published in its final form. Please note that during the production process errors may be discovered which could affect the content, and all legal disclaimers that apply to the journal pertain.

Although reasonable efforts have been made to obtain all necessary permissions from third parties to include their copyrighted content within this article, their full citation and copyright line may not be present in this Accepted Manuscript version. Before using any content from this article, please refer to the Version of Record once published for full citation and copyright details, as permissions may be required.

## The Red Sea rifting in central Egypt: constraints from the offshore Quseir

Moamen Ali<sup>1, 2, 3</sup>, Alessandro Decarlis<sup>1,2</sup>, Marco Ligi<sup>4</sup>, Philip Ball<sup>5</sup>, William Bosworth<sup>6</sup> and Andrea Ceriani<sup>1,2</sup>

<sup>1</sup> R.I.C.H. Center: Research and Innovation on CO<sub>2</sub> and H<sub>2</sub>, Khalifa University of Science and Technology, P.O. Box 127788, Abu Dhabi, UAE.

<sup>2</sup> Earth Sciences Department, Khalifa University of Science and Technology, P.O. Box 127788, Abu Dhabi, UAE.

<sup>3</sup> Department of Geology, Assiut University, Assiut, Egypt.

<sup>4</sup> Istituto di Scienze Marine, CNR, Via Gobetti 101, 40129, Bologna, Italy.

<sup>5</sup> Keele University, Faculty of Natural Sciences, Geography, Geology and the Environment, William Smith Building, Newcastle ST5 5BG, UK

<sup>6</sup> Apache Egypt Companies, 11 Street 281, New Maadi, Cairo, Egypt

\* *Corresponding author, Email: momen.mohamed@science.au.edu.eg* ORCID: 0000-0002-5625-5390

### Abstract:

Southern and Central Red Sea oceanic crust formation is generally accepted to have started ~5 Ma. However, the nature of the crust in the Northern Red Sea (NRS) is still debated. This paper describes the rift architecture, dynamics and evolution of the NRS and identifies domains that relate to first-order geodynamic processes. The proximal margin domain is located onshore and is characterized by latest Oligocene-Miocene half-graben basins. New seismic interpretations show that the offshore region is a necking domain dominated by low angle, high offset extensional faults, which led to the exhumation of lower crustal gabbros at Brothers Islands. 2D forward models suggest that necking passes into a distal margin domain, where the continental crust thins to < 10 km at 120 km from the coast. Sensitivity testing of interpretations for the distal domain indicates a probable scenario where exhumed lower continental crust or serpentized mantle is present. A comprehensive rift model for the NRS in the Quseir sector accounts for circa 25 Ma magmatic underplating accompanied by half-graben development, followed by Early Miocene crustal thinning accommodated by an east-dipping detachment fault, and a Late Miocene phase with a flip of the detachment geometry, that led to the present-day configuration.

**Keywords:** Northern Red Sea, Magma-poor rifting, Necking domain, Mantle exhumation, Flip-flop detachments, Brothers Islands

## Introduction

The evolution of rifted margins can be described using a rift domain classification if the data and observation are sufficient to allow their identification. Ideally, this relies on high-quality seismic, stratigraphic, or outcrop exposures. Detailed analysis is possible in some fossil margins, for example, the Pyrenees and Alpine Tethyan margins (Mohn *et al.* 2012; Masini *et al.* 2013; Decarlis *et al.* 2017; Ribes *et al.* 2020), or in offshore regions where the seismic data quality allows such as Newfoundland, Bay of Biscay, Angola (e.g., Sutra *et al.* 2013; Tugend *et al.* 2014; Lavier *et al.* 2019; Martinez *et al.* 2021). Furthermore, numerical modeling exploring the distribution of the syn- and post-rift sequences in space and time can be used to analyze and map the tectonic evolution of the basins and rifted margins (Pérez-Gussinyé *et al.* 2020). Numerical models have been applied to study rifted margins in South China Sea, Pyrenees, North Atlantic, and South Atlantic (Capitanio *et al.* 2020; Chenin *et al.* 2020; Duretz *et al.* 2020; Pérez-Gussinyé *et al.* 2020; Li *et al.* 2021). Today it is generally accepted that the different rift domains exhibit geodynamic processes characterized by specific sedimentological, fluid, magmatic and structural characteristics (Jagoutz *et al.* 2007; Sutra *et al.* 2013; Pinto *et al.* 2014; Chenin *et al.* 2015; Manatschal *et al.* 2015; Picazo *et al.* 2016; Sinadinovski *et al.* 2017; Incerpi *et al.* 2020).

The Red Sea is a young rifted margin. Extension relating to the Red Sea rift system initiated in the Late Oligocene-Early Miocene (25-23 Ma) and led to the separation of the present-day Nubian and Arabian shields (Fig. 1; Cochran 1983; Joffe and Garfunkel 1987; Coleman 1993; Bosworth and McClay 2001). The basin's shape, bathymetry and rift shoulders resulted from a complex polyphase tectonic evolution. The study area of this paper is located in the Northern Red Sea (NRS) and spans roughly from 25° N to 27° N (Fig. 2). GPS data confirm that the Arabian and African plates are drifting apart with an average rate of  $1.7 \pm 0.1$  cm/yr in the South of the Red Sea region, decreasing to  $0.7 \pm 0.1$  cm/yr in the NRS (ArRajehi *et al.* 2010; Reilinger *et al.* 2015). The direction of extension is thought to have varied at different times in the Red Sea's evolution. Initial rift phases were orthogonal to the rift axis (approx. ENE) indicated by the alignment of the deeps and later changing into oblique extension (NNE) since the activation of the Dead Sea transform in the Middle Miocene (Lyberis 1988; Bosworth and McClay 2001; Bosworth *et al.* 2005; ArRajehi *et al.* 2010).

The nature of the crust along the axis of the Red Sea remains highly debated. Several studies concur that the southern and central sectors are rifted margins that reached or approached the oceanic stage. Evidence for continuous or punctuated oceanic ridges was

found, and cruise campaigns sampled ocean floor basalts at different sites between 17° N and 19° 30' N (Bonatti 1985). In these areas, the maximum age for the oceanic crust was dated 5 Ma (Cochran 1983; Bonatti 1985; Cochran and Karner 2007), while some axial structures, interpreted as isolated ridge segments in the central Red Sea (Thetis and Nereus deeps), contain 3 to 1 Ma old crust (Fig. 1; Ligi *et al.* 2011, 2012). Towards the north, where a proper ridge-like morphology is lacking and linear magmatic anomalies are absent, determining the nature of the crust is problematic. The crust under the NRS has been reported to be either oceanic crust (e.g., Girdler and Underwood 1985; Gaulier *et al.* 1988; Augustin *et al.* 2021; El Khrepy *et al.* 2021), or as a region of hyperextended continental crust punctuated by volcanic deeps, sometimes interpreted as nascent ridges (Bonatti 1985; Cochran 2005; Cochran and Karner 2007; Ligi *et al.* 2012, 2018; Mahsoub *et al.* 2012; Mitchell and Park 2014; Almalki *et al.* 2015; Sinadinovski *et al.* 2017; Keller *et al.* 2018; Stockli and Bosworth 2019; Le Magoarou *et al.* 2021).

This study aims to describe the first-order architecture of the Egyptian margin in the NRS at the latitude of Quseir and to analyze its geometric evolution based on an original interpretation of different geophysical datasets, a review of literature on outcrop geology, and a domains-driven comparison with other similar modern margins worldwide. We have developed a rift domain model based on observations of structural elements in seismics, including in their evolution the interaction with the magmatic activity. Results lead to a conceptual model of extension for this part of the NRS.

### **Stratigraphic and structural framework of the Egyptian margin**

Traditionally the geological record of the NRS has been subdivided into two primary tectonostratigraphic sequences (Fig. 3; Hughes and Beydoun 1992; Patton *et al.* 1994; Khalil and McClay 2001; Hughes and Johnson 2005). Most of the information on the sequences comes from onshore stratigraphic data and offshore well-log data: (i) Pre-rift sediments: formed by the igneous and metamorphic basement and Late Cretaceous to Eocene sedimentary rocks, (ii) Syn-rift sequence: subdivided into an early and a late-syn-rift section. The early syn-rift sediments include Late Oligocene-Early Miocene sediments underlying the red beds of the Nakheil and Abu Ghusum Formations in the onshore area and the Abu Zenima Formation in the offshore region of the Egyptian Red Sea margin (Fig. 3). The late syn-rift sequence is mainly composed of Early to Middle Miocene clastic rocks and Middle to Late Miocene massive halite and layered evaporites, followed by Plio-Quaternary siliciclastic sediments (Fig. 3). The paucity of high-quality, long-record and long-offset multi-channel

seismic reflection data, coupled with limited well data, means that the geological evolution of the Red Sea remains obscure. Furthermore, the seismic image of the Red Sea is hampered due to the presence of shallow carbonates and allochthonous evaporite sequences, which leads to difficulties in determine the stratigraphy (Masini *et al.* 2020) and in understanding the structure and nature of the crust in the distal margin regions (Ball *et al.* 2018a, b; Le Magoarou *et al.* 2021).

Several studies have examined the onshore domain of the NRS using classical field techniques (e.g., Jarrige *et al.* 1990; Bosworth *et al.* 1998, 2020; Plaziat *et al.* 1998; Khalil and McClay 2001, 2009; Moustafa and Khalil 2020). The offshore domain has only been described using geophysical data and the available commercial borehole data or analytical results of seabed samples recovered by dredging from the axial domains (Tewfik and Ayyad 1982; Miller and Barakat 1988; Gordon *et al.* 2010; Mitchell *et al.* 2017; Ligi *et al.* 2018; Bosworth *et al.* 2020). Onshore studies indicate that sedimentary rocks were deposited inside a number of km-scale basins bounded by major, high-angle, NW-SE striking extensional faults (Fig. 2; Tewfik and Ayyad 1982; Montenat *et al.* 1988; Jarrige *et al.* 1990; Patton *et al.* 1994; Khalil and McClay 2001, 2009). The strike of the master fault system is roughly parallel to the Red Sea rift axis (NW direction). The northwestern coast of the Red Sea includes two structural provinces, Quseir and Safaga, characterized by numerous km-scale half-graben basins with an opposite dip of the master faults (Jarrige *et al.* 1990; Bosworth 1994). The southern province (Quseir) comprises half-graben structures bounded by faults striking NW-SE but dipping to the SW (e.g., Zug El Bahar, Hamadat, and Duwi fault blocks, Fig. 2). The dominant fault polarity and half-graben geometry changes at the Duwi accommodation zone (DAZ), also known as Duwi-Quseir-Brothers (Jarrige *et al.* 1990; Bosworth 1994; Moustafa 1997; Khalil and McClay 2001, 2009; Younes and McClay 2002). In the northern sector (Safaga), the faults bounding the NW-SE trending half-grabens dip to the NE (e.g., Um El Huetat, Wasif and Rabah fault blocks; Khalil and McClay 2009). The Safaga province is contiguous with the Amal-Zeit province of the Gulf of Suez (Bosworth *et al.* 2020), while the DAZ was probably connected to the Duba accommodation zone in Saudi Arabia during the early-rift phases (Figs. 1 and 2; Bosworth 1994; Bosworth and Burke 2005).

Offshore, studies have focused on low-quality, single-channel seismic reflection data, where a number of reflectors have been described in the shallow Pliocene to Recent sediments. In particular, a major unconformity surface between the Upper Miocene layered evaporites and the Plio-Quaternary sequence (S-reflector) was identified along with

numerous irregular salt domes and prominent salt walls, which are often associated with complex fault patterns, especially close to the bathymetric deeps (Girdler and Whitmarsh 1974; Mitchell *et al.* 2010, 2017, 2019). Based on these studies, the structural pattern of the Egyptian offshore margin is similar to that of the southern part of the Gulf of Suez, and it is characterized by a NW-SE fault system parallel to the NRS rift axis (Fig. 2; Tewfik and Ayyad 1982; Barakat and Miller 1984). Moreover, the structural setting of the NRS was affected by the formation of the Dead Sea transform that accommodated a northward displacement of the Arabia plate relative to the Sinai sub-plate. Several phases of left-lateral shear have been recognized distributing along the Gulf of Aqaba to the Maras Triple Junction, SE Turkey. These phases were active from the Mid-Late Miocene (~14 Ma) to the present day, with a prominent post-Pliocene pulse that propagated in the northern Red Sea (Quennell 1951, 1958; Girdler 1990; Bosworth and Burke 2005).

A few important offshore outcrops in the NRS are preserved at the Brothers Islands (gabbros; Ligi *et al.* 2018) and Zabargad Island (peridotites, gabbros, metasediments and sedimentary rocks; Bonatti *et al.* 1986) (Fig. 4a). Geochemistry of the Brothers gabbros suggest a MORB-type (mid-ocean ridge basalts) origin for the parental melt that crystallized at  $25 \pm 6$  Ma ( $^{40}\text{Ar}/^{39}\text{Ar}$ ; Ligi *et al.* 2018). Consequently, the Brothers gabbros are interpreted as lower crustal intrusions of asthenospheric melt emplaced in the first phase of rifting, subsequently exhumed above the sea level due to a significant uplift of an extensional fault footwall (Ligi *et al.* 2018).

The identification of detachment faults along the Red Sea is limited to a few works in the literature (Wernicke 1981; Voggenreiter *et al.* 1988; Ball *et al.* 2018a, b; Keller *et al.* 2018; Stockli and Bosworth 2019; Masini *et al.* 2020), where it is argued that detachment surfaces, interpreted by seismic data, are overlain by the Middle Miocene evaporites (15-11 Ma) and that the halite deposition is contemporaneous with the exhumation of lower crust and mantle. The evolution of high and low-angle fault systems is documented in isolated examples where data or field accessibility is good. Such observations can help build an understanding of plate kinematics evolution during Red Sea rifting. However, the identification of detachment systems in the Red Sea has been limited due to the lack of access to deep, high-quality seismic data.

## Data and methods

Different geophysical data were used to study the central part of the Egyptian Red Sea and unravel the margin's architecture (Fig. 4). Magnetic and gravity datasets, covering the

entire Red Sea onshore and offshore, were used to integrate interpretations of the 2D and 3D seismic data in offshore Quseir and extend interpretations to a regional scale.

#### *Seismic and well data*

The 2D seismic data include five industry seismic reflection profiles from three surveys with a total length of about 412 km and depth imaging ranging from 5 to 6 seconds two-way travel time (TWT). The 2D seismic sections were acquired by Esso Red Sea (ERS) and Philips Red Sea (PRS) companies between 1975 and 1977. The 3D seismic survey was acquired in 1999 by British Gas and covered 1600 km<sup>2</sup> offshore central Egypt between Safaga and Quseir and west of Brothers Islands (Fig. 4b; Gordon *et al.* 2010). The survey includes 4879 crosslines in the NE-SW direction with 12.5 m spacing, and 1729 inlines trending NW-SE with a spacing of 25 m. The 3D data allows imaging down to 7 s TWT. Borehole data are from four wells: RSO-B 96-1, RSO-B 95-1, Quseir A-1X, and Quseir B-1X (see Fig. 4b for locations). All the wells penetrated the basement except RSO-B 95-1, which terminates in the Early Miocene Rudeis Formation at 4022 m (Fig. 4b). The seismic interpretation procedures included seismic-to-well ties, fault delineation, and picking primary seismo-stratigraphic sequences in the study area (Figs. 5-7; Ali *et al.* 2018, 2020, 2022c; Ali 2020). Average interval velocities were adopted in the time-to-depth conversion of the interpreted seismic sequences to generate the 2D forward models (Table 1).

#### *Gravity and magnetic data*

The Bouguer gravity data were obtained from the WGM2012 global gravity model (Bonvalot *et al.* 2012), which derive from the Earth global gravity models EGM2008 and DTU10 corrected (using a reference density of 2670 kg/m<sup>3</sup>) for surfaces masses contributions based on the 1 arc-minute global relief model ETOPO1 (Balmino *et al.* 2012). Free-air gravity data of the study area were extracted from the satellite-derived global grid (version 31) of Sandwell *et al.* (2014) and a free-air gravity anomaly map was generated with a grid resolution of 1 arc-minute (about 1.852 km) over an area of 175x175 km (Fig. 8a). Gravity-field accuracy derived from satellite altimetry depends on altimeter range precision, spatial track density and different track orientation. The current version of the altimeter-derived gravity field has an accuracy of about 1-2 mGal with improvements mainly in the 12 to 40 km wavelength band that is of interest for studying structures up to 6 km. A Bouguer gravity profile in the NE-SW direction was extrapolated along ERS-26 and PRS-72 seismic lines and extended northeastward to the rift axis with a total length of 155 km to perform 2D forward models (see Fig. 8 for location). A total magnetic intensity map (TMI) of the study area was generated extracting data from the EMAG2<sub>v3</sub> global database provided by (Meyer *et al.*

2017) with a grid resolution of 2 minutes (about 3.74 km). Magnetic anomaly values are evaluated at the reference elevation of 4 km, and each grid value comes with an error estimate (Meyer *et al.* 2017). Reduced to the Pole (RTP) filter was applied on the TMI map of the study area to remove the effect of induced magnetization and strike on the shape of magnetic anomalies (Fig. 8b; Keating and Zerbo 1996; Cooper and Cowan 2005; Li 2008). A NE-SW RTP profile crossing the Egyptian margin with a length of 155 km was extrapolated to construct the 2D forward models.

### *Forward modelling*

The GM-SYS profile tool of the Oasis Montaj® software was used to develop the forward modelling. The interpreted seismic units, time-to-depth converted and calibrated with the well stratigraphy, were included in the modelling, i.e., the Plio-Quaternary sediments, the layered evaporites, the massive halite, the pre-salt syn-rift sediments and the pre-rift seismic basement (Fig. 9). Adopted magnetic susceptibilities and densities of the seismic sequences derive from average values taken from the literature (Table 1).

- A first set of gravity and magnetic forward models was realized to verify and refine the proposed tectonic and stratigraphic architecture of interpreted seismic profiles. The modelled section is 95 km long and includes an onshore part, whose stratigraphy is taken from the literature (e.g., Gaulier *et al.* 1988; Khalil and McClay 2002, 2017, 2020), and an offshore segment inferred from the seismic interpretation (Fig. 5).
- The second set of models was generated including an extrapolated 60 km-long distal segment (no public or industrial seismic data are available). The segment is an extension of the previous model towards the Red Sea axial trough. Several models with simplified crustal structures have been tested, and three end-members were identified for the distal part: i) exhumation of lower crust (Fig. 9); ii) mantle exhumation (Fig. 10); and iii) seafloor spreading initiation with accretion of oceanic crust (Fig. 11).

During each simulation, parameters were adjusted to approach the best fit between the calculated gravity and magnetic values until observed anomalies were achieved.

## **Results**

Results from the seismic interpretation, magnetic anomalies, free-air gravity anomalies, and forward modelling are discussed in detail in the following sections.

### *Seismic interpretation*

A number of seismo-sedimentary packages (or sequences) have been recognized to

guide interpretation, using geometry of reflectors, seismic attributes and seismic facies analysis, and literature as discriminants (e.g., Ligi *et al.* 2018). The stratigraphic framework of the onshore geology, as identified by Khalil and McClay (2002, 2009), has been tentatively correlated with the distal NRS margin to constrain the tectonic evolution of the basin. The presence of a widespread thick evaporitic layer hampers the penetration of the seismic signal and limits the sharpness of deeper seismic horizons. Nevertheless, the top of the crystalline basement is usually well imaged because highly reflective and is distributed within a depth (TWT) ranging from 1.4 s to 4.3 s (S1 in Figs. 5-7). The considerable depth variation reflects the significant effectiveness of normal faults which crosscut the basement (e.g., the low-angle east-dipping F1 fault, Fig. 5). In addition, the study area is characterized in the central and northeastern sectors by two prominent basement highs (Fig. 5) formed by two large-throw low-angle west-dipping normal faults (F2, F3 in Fig. 5). The basement approaches the seafloor at these locations with the easternmost one corresponding to the submarine continuation of the Brother Islands high. The basement shows convolute reflectors and layered zone without a preferential arrangement, however the volume appears to be relatively homogenous and no significant differences or sharp zonations can be distinguished. Zones of thin layering can be distinguished locally close to top of the basement. These reflectors can be locally interpreted as part of the pre-rift successions (S2 in Fig. 7), locally tilted and arranged in blocks limited by normal faults with an offset of a few milliseconds. Sometimes the interpretation is uncertain especially in depth, due to the poor seismic illumination that does not permit to follow reflectors sideways. In the central part of the interpreted seismic section (Fig. 5), some sharp reflectors form a wedge with evidence of a significant thickening toward northeast (S3 in Fig. 5). The growth of this unit is significant approaching the master fault F2. It is also evident that this early syn-rift S3 sequence is not present northeast of the two basement highs (Fig. 5).

The pre- (S2) and early syn-rift (S3) deposits are followed upward by a thick sequence of reflective layers with low to moderate amplitudes (S4 in Figs. 5-7). This interval is characterized by several normal faults with small throws (around a few ms TWT) and a considerable variability in thickness ranging from 0.25 to 1.8 s (TWT, roughly 340-2150 m). The entire sequence is gently tilted seaward and folded in the area adjacent to the westernmost basement high in the central portion of the seismic section (Figs. 5 and 7). This sequence is interpreted as a clastic, moderately-layered syn-rift sedimentary sequence. This unit is post-tectonic in relation to both F1 and F2 faults, while it is probably pre-tectonic relative to F3 because S4 deposits are strongly inclined on the hanging-wall side following

tilting of the fault block (Fig. 5). The syn-rift sequence is overlain by a low reflectivity unit with no internal coherent reflections leading to a complex and chaotic seismic facies (S5 in Figs. 5-7). This sequence is attributed to a thick layer of massive salt (Ligi *et al.* 2018) that seals most of the normal faults cutting the pre- and syn-rift sediments (Figs. 5-7). It is widespread along the imaged margin, with a thickness ranging between 0.1 and 1.2 s TWT (roughly 200-2500 m). Halite forms typical halokinetic structures, such as km-scale diapirs and salt walls (Figs. 5-7). The salt domes gradually disappear in the easternmost sector of the study area and give way to a poorly to moderately stratified unit with low-medium amplitude reflectors in the basin located between the two structural highs (Fig. 5). Its presence toward the rift axis beyond the easternmost high cannot be confirmed, and it may be only hypothesized (Fig. 5). The mobilized halite is followed by a sequence with moderately to well-stratified reflectors having from moderate to high amplitudes. This unit is interpreted as consisting of layered evaporites (S6 in Figs. 5-7). Reflectors are tilted and folded due to the halokinetic activity resulting in large variability in the sequence thickness. The thickest sections are found in the mini-basins formed between salt diapirs/walls with thicknesses ranging from 0.5 to 1.5 s TWT (roughly 820-2500 m), while the thinnest are observed directly above the tops of the salt diapirs/walls (Figs. 5-7). In the basin between the distal basement highs, the layered evaporites appear to be syn-tectonic with respect to the movement along the fault F3. Close to the present-day shoreline, reflectors of the layered evaporites down-lap the crystalline basement creating an unconformity surface (Fig. 5b).

The top of the layered evaporites unit is marked by a characteristic reflector present in the entire NRS, known as S-reflector (Ross and Schlee, 1973). This high amplitude, sharp and well imaged reflector represents a major unconformity between the Late Miocene evaporites and Pliocene sedimentary rocks (Figs. 5-7). Above, the Plio-Quaternary sequence (S7 in Figs. 5-7) appears well stratified with parallel to subparallel reflectors having medium to high amplitudes. The thickness of this unit is extremely variable ranging from 0.16 to 1.4 s TWT (roughly 150-1350 m) due to the differential subsidence caused by the combined action of salt tectonics and pre-existing topography. In addition, a recent large igneous body, interpreted as a volcanic complex with density (up to  $2.65 \text{ g/cm}^3$ ) and magnetic susceptibility of  $3400 \mu\text{cg}$ s (Ali *et al.* 2022a, b), was located on the top of the westernmost distal basement high at the footwall of F2. Similarly, about 8 km northeast at Brothers Islands, a second high-density body is interpreted as a large gabbroic block probably intruded by the same recent magmatic events (Fig. 9).

Several normal faults penetrating the crystalline basement have been interpreted using

the available seismic data. The Middle-Late Miocene (15-5.3 Ma) evaporites seal these faults. A different group of normal faults is observed passing through the layered evaporites and Plio-Quaternary sections. The normal faults show large throw variations from a few ms up to 3 s (TWT) forming graben, half-graben and horst structures (Figs. 5-7).

#### *Gravity and magnetic interpretation*

The free-air gravity anomaly map for the study area shows values ranging between -40 and 40 mGal. The Egyptian onshore area is characterized by a generalized positive anomaly, with growing values towards the Red Sea Hills region, in the SW. Along the coast, it is possible to observe the passage to an elongated anomaly characterized by highly negative free-air values  $>-30$  mGal. These anomalies probably mark the sharp passage between an area characterized by thick continental crust (onshore Quseir) and a sector characterized by thick sedimentary basins that likely deposited on a thinned crustal section (necking zone). The offshore area is generally characterized by a slightly negative "background" anomaly (-10/-20 mGal) with negative and positive local peaks. The latter, with more than 30 mGal, are observed around and off Brothers Islands; they are aligned in the NE-SW direction and have elongated shapes trending SE-NW parallel to the rift axis (Fig. 8a). These anomalies have been interpreted as recent volcanic edifices (Cochran and Karner 2007; Duncan and Al-Amri 2013; Ali *et al.* 2022a, b). The RTP map with a contour interval of 75 nT shows values ranging between -175 and 225 nT (Fig. 8b). The onshore area shows local positive anomalies with magnetic values ranging from 15 to 65 nT corresponding to the Red Sea Hills, while the offshore area displays two significant negative anomalies (-80 to -175 nT). At least seven significant positive magnetic anomalies are observed offshore Quseir along the axial trough and off-axis. They show high positive magnetic values ranging between 75 and 225 nT and are interpreted as magmatic buildups (e.g., Ali *et al.* 2022a, b; Fig. 8b). The large anomaly southwest of the Brothers Islands is surrounded by a negative anomaly that corresponds to a sharp magnetic susceptibility contrast between the seamount and the surrounding sedimentary deposits.

#### *2D Forward modelling*

Different 2D forward models were analyzed to propose and discuss different crustal architectures for the NRS (Figs. 9-11) along a ~155 km-long NE-SW line, perpendicular to the rift axis in the central part of the study area. The modelled section consists of an onshore sector, crossing the Gebel Hamadat and Wadi Hamadat localities south Quseir and an offshore part that follows the interpreted seismic lines shown in Fig. 5 that run from the

Quseir coast to the rift axis crossing the Brothers Islands structural high (Fig. 8). The models investigate a lithospheric section up to a maximum depth of 36 km. The geometry of the western and central sectors of the models derives from seismic interpretation, field data and previous literature (about 95 Km from the western origin). The modelled section includes six lithological units, from bottom to top: asthenosphere, mantle, lower crust, middle crust, upper crust and sedimentary cover. Based on the seismic interpretation, the sedimentary cover is divided into seven stratigraphic units each with specific values of density and magnetic susceptibility assumed on the basis of average values of their petro-physical characteristics (Figs. 9-11). In addition, two volcanic complexes (basalts) are included at the top of the distal basement highs to simulate recent volcanic activity, as proposed by Ali *et al.* (2022a, b).

The easternmost geological section, about 60 km-long, is purely speculative and was introduced to verify the gravimetric and magnetic response of some hypotheses on the crustal structure of the most distal portion of the margin (i.e., exhumed crust, exhumed mantle and oceanic crust; Figs. 9-11).

- The geological model in Fig. 9 simulates a scenario in which the rifted margin is composed only of continental crust, covered by a thick salt layer and layered evaporites up to the rift axis. Based on seismic refraction data, the seismic velocities below the NRS axial trough range from 5.53 to 6.38 km/s (Gaulier *et al.* 1988) suggesting the presence of continental crust at the rift axis, although small areas with higher density and seismic velocity have been observed, probably due to mafic intrusions. A view in line with a NRS rift model suggested by several authors (Cochran 1983, 2005; Bonatti 1985; Bosworth *et al.* 1993; Mahsoub *et al.* 2012; Mitchell and Park 2014; Almalki *et al.* 2015; Ligi *et al.* 2018; Le Magoarou *et al.* 2021).

The Moho depth, obtained by iteratively adjusting its depth through the best fit between the predicted and measured gravity and magnetic anomalies, is consistent with what is reported in the literature (Mooney *et al.* 1985; Voggenreiter *et al.* 1988; Hosny and Nyblade 2014, 2016; Tang *et al.* 2016). The Moho lies at a depth of about 32 km beneath the Quseir onshore and dramatically rises to shallower levels with a crustal thickness of ~20 km near the coast decreasing to 6-8 km at the rift axis (Fig. 9). Ligi *et al.* (2018) described gabbroic rocks sampled from the top of Brother Islands with an  $^{40}\text{Ar}/^{39}\text{Ar}$  age of 25 Ma having a probable lower crustal origin. Thus, the F3 fault, whose footwall block forms the Brothers' high, was assumed to partially correspond to the tectonic boundary between upper and lower crust (Fig. 5). The

halite sequence is distributed over the entire area, with a thickness varying from less than 100 m in the welded areas and 2500 m in the salt diapirs/walls (Figs. 5 and 9). The best fit between the predicted and measured potential data was achieved extending the thick halite sequence ( $>2.4$  km;  $2100$  to  $2250$   $\text{kg/m}^3$ ) directly above the lower crust ( $2800$   $\text{kg/m}^3$ ) northeast of Brothers Islands. The comparison between the predicted and measured gravity and magnetic anomalies shows a good fit for the southwestern portion of the model section (first 95 km) with negligible error due to the excellent control from the seismic data. Conversely, the distal part (from 95 km to 155 km) displays large errors especially in the region comprises between 100 and 125 km. The total error between the predicted and measured gravity and magnetic data is 7.03 mGal and 13.85 nT, respectively (Fig. 9a and b).

- In the model of Fig. 10, exhumation and serpentinization of upper mantle is hypothesized. This scenario is suggested by the sharp decrease in the measured Bouguer anomaly northeast of Brothers Islands (Fig. 10a and b). Thus, between km 92 and 140 of the model section, a mantle body of serpentinized peridotites was introduced to replace the lower crust of the previous model and the overlying halite sequence was reduced in thickness up to 2 km. The density of the serpentinized mantle was assumed to vary upwards from  $2650$  to  $2500$   $\text{kg/m}^3$  to simulate an increase of serpentinization towards the top of the body. Results from this model shows the best match between predicted and measured gravity and magnetic data with errors reduced to 2.52 mGal and 7.26 nT (Fig. 10a and 10b).

- The model of Fig. 11 includes the hypothesis of the presence of oceanic crust below the NRS axial trough (Girdler and Underwood 1985; Gaulier *et al.* 1988; Augustin *et al.* 2021; El Khrepy *et al.* 2021). Between km 108 and 120 of the model section, a 3 km-thick slab of oceanic crust with a density of  $2900$   $\text{kg/m}^3$  was introduced to simulate a possible magmatic crustal accretion at the rift axis, i.e., seafloor spreading initiation. In order to reduce the errors between predicted and measured values, oceanic accretion was assumed to have started after mantle exhumation with two serpentinized mantle bodies flanking the oceanic crust. Results from the forward model C displays the largest dis-matching between the calculated and measured gravity and magnetic data (more than 50 mGal and 60 nT). While the total error for the magnetic curve is 34.35, the gravity curve shows a total error of 26.72 (Fig. 11).

## Discussion

### *Rifted margin domains*

Based on the literature, seismic interpretation and 2D forward modelling, a first-order zonation of the NRS Egyptian margin can be recognized using the proposed crustal thicknesses, distribution of sediments and fault kinematics as discriminants. Our analysis follows the rift domains classification of magma-poor rifted margins introduced in the last decade (Tugend *et al.* 2014; Gillard *et al.* 2015). These models derive from direct observations of paleo-rifted margins in orogenic systems such as Pyrenees and European Alps and from the analysis of modern margins such as Iberia-Newfoundland and Eastern India (e.g., Manatschal 2004; Sutra and Manatschal 2012; Mohn *et al.* 2015; Hauptert *et al.* 2016).

The onshore area of the proposed section (Fig. 10) is characterized by a thick crustal section (30-32 Km). On the surface, a widespread metamorphic basement is affected by a prominent system of graben and half-graben basins active since the first phases of rifting. The basin infills consist of relatively thin, shallow water to continental sedimentary deposits. The Duwi, Hamadat and Zug El Bahar half-grabens represent the major basins of the Quseir region (Fig. 12; Khalil and McClay 2002, 2020). The analysis of the sedimentary sequences allows to distinguish a Cretaceous-Middle Eocene pre-tectonic (Duwi Formation, Esna and Dakhla Shale, Thebes Formation) and a Late Oligocene unit (Nakheil Formation). Miocene sedimentary rocks are not present in the onshore basins (Fig. 12c); while a Plio-Quaternary sequence, the oldest observable post-tectonic unit, lies unconformably on the Late Oligocene rocks. Basins are generated by several NW trending faults, dipping to the SW in the Hamadat half-graben and abruptly changing to the NE along the Duwi accommodation zone (DAZ) (Fig. 12b). The half-graben basins on the Egyptian margins correlate exceptionally well with an analogous one in the onshore Saudi Arabia, once retro-deformed to accommodate a late-rifting left-lateral strike-slip movement (Bosworth 2015). This sector is compatible with the *proximal margin* described by Tugend *et al.* (2014), which in several examples of modern and fossil margins shows evidence of widespread extensional basins, mostly half-grabens, distributed over belts several hundred-km wide. The extension is localized in the upper crust, and the  $\beta$  factor is usually quite limited ( $<1.5$ ). The proximal margins are characterized by thick continental crust, they are extended during the first phase of rifting only, and then they become quiescent as the thinning process becomes active, and tectonics start to be focused towards the distal sector (stretching phase: e.g., Sutra *et al.* 2013).

A significant change in the architecture of the Red Sea margin can be observed close to the present-day shoreline. A large negative anomaly elongated in the NW-SE is observed

from the free-air gravity map, showing values ranging from -20 to -40 mGal localized into a 25 x 84 km-wide area (necking zone; Fig. 8a). This anomaly marks the presence of a deep sedimentary basin elongated parallel to the coast, as evidenced by the interpretation of seismic line PRS-72 (Fig. 5b). In addition, the 2D forward modelling shows that the anomaly can be explained by a significant thinning of the crust seaward and that this transition occurs beneath the present-day shoreline (Fig. 10). The formation of the *necking zone* due to the hyperextension process started probably during the Early Miocene. The crust thins eastward from 32 km below the Quseir onshore to about 22 km beneath the necking domain (Fig. 10). A peculiar field evidence constrains the geophysical data: onshore Miocene evaporites are recognized only along the coast and are absent in the Red Sea Hills. This may be due to syn-rift uplift and erosion of the Egyptian margin or to non-deposition. Nevertheless, given that the Miocene deposits are found only near the coast and offshore, it implies that these sectors continuously subsided during rifting (Fig. 12c).

Conversely, locating the early rift half-graben structures offshore is difficult because the offshore structural framework is dominated by east-dipping, low-angle and large-offset normal faults (Stockli and Bosworth 2019). Seismic interpretation highlights a prominent east-dipping detachment fault in the study area (F1, Fig. 5). In addition, the F2 fault probably represents the distal continuation of the same structure, *i.e.*, the rolling hinge isostatic uplift of the same system. The S3 syn-tectonic sequence is unique and was deposited during the formation of the detachment fault, probably above hanging walls of a set of domino-arranged blocks (Fig. 5). This sector of the margin can be compared with the *necking zone* and the passage to the *distal margin* of Tugend *et al.* (2014). Distal margins of several magma-poor rifts (Masini *et al.* 2013; Decarlis *et al.* 2015) show thinned to ultra-thinned continental crust and high  $\beta$  factor values ( $>1.5$ ). A distal margin develops during the seaward migration of the deformation and it is characterized by a specific syn-tectonic sedimentary sequence (cfr. STS2 in Decarlis *et al.* 2015). In the NRS, this sequence can be represented by the deposition of the massive salt and layered evaporites. Seawards, we interpret the distal margin as the sector showing an extreme crustal thinning from 22 km in the necking zone to less than 10 km (Fig. 10). Seismic interpretation indicates that the allochthonous to semi-allochthonous, salt diapirs/walls are restricted only to the distal margin with no evidence of salt domes at the necking domain. Moreover, several reflectors with high amplitudes observed within the distal margin basement are interpreted as gabbroic underplated bodies (Figs. 5-7).

Following our interpretation, the Egyptian margin at Quseir is mainly formed by a continental crust wedge resting in the footwall of a low-angle, high-throw normal fault, in

which the basement was exposed at the seafloor and affected by slow but continuous subsidence. The hanging wall, or upper plate, of this system, is probably preserved on the conjugate margin in the Arabia plate. For this reason, following the margin nomenclature (Sutra *et al.* 2013; Tugend *et al.* 2014; Gillard *et al.* 2015), we infer that the Quseir margin represents the lower plate and that of Saudi Arabia the upper plate of the rift system (Fig. 13b). The interpreted F3 fault represents a subsequent (younger) west-dipping detachment fault. In fact, it is possible to determine that this fault originated in an advanced stage of rifting by observing the seismo-stratigraphic units involved in the fault movement. The activation of the F3 detachment probably occurred only during the deposition of the halite sequence or even later (Upper Miocene?), because the F3 cuts the footwall of the previous detachment faults F1 and F2 (Fig. 13c). In addition, gabbroic rocks outcropping at Brothers Islands (Ligi *et al.* 2018) suggest that the footwall of F3 is probably made up of exhumed lower crust. A sequence of events that can be related to the development of flip-flop structures, as those observed in oceanic domains *s.s.* and in continental settings (Geoffroy *et al.* 2014).

#### *Rifting Model:*

Proposing a rift model for the NRS is challenging because of the few data available in comparison to other rift systems and even in the case of margins with complete and high-quality databases it may lead to different models (e.g., Brazilian offshore: see Karner 2000; Karner *et al.* 2021). A holistic approach is required to overcome the lack of good seismic data and the paucity of wells/sampling. The comparison with geometries proposed in other margins may help. The above-described rifting domain classification is inspired and driven by models developed at magma-poor margin but can be critically applied to system with different amounts of magmatic additions. The proposed geometry of the Egyptian margin at Quseir seems to fit quite well with that of the Australian margin line GA199 described in Gillard *et al.* (2016), interpreted as a lower plate located at the footwall of a seaward dipping major detachment fault system. In the Australian example, the isostatic rebound led to the uplift and over the tilt of the tip of the margin, generating the narrow and elongated basin that rests onto the necking zone, a feature that can be seen in the Egyptian margin as well. The difference between the two examples is that the Australian margin continued to extend, reaching the mantle exhumation stage and the development of successive detachments (and complex flip-flop systems) in the most distal domain, while in the Egyptian rift kinematics appear to have changed early after the exhumation of the lower crust and mantle during the

Late Miocene, changing to a complex trans-tensional component, as a result of the onset of the Dead-sea transform (e.g., Bosworth and Burke 2005). The change in kinematics of the early rifting evolving to oblique rifting in the NRS is a limitation when considering a direct comparison with the Brazilian offshore Pelotas/Campo/Santos Basins. The younging of basement presented by Karner *et al.* (2021) is interesting, and there may be similarities to draw in the NRS. Another similarity worth considering is the fact that evaporites are present along both margins.

When comparing the Brazil and NRS margins the first order approach described by Zalán (2017) and revised by Karner *et al.* (2021) may offer a template for rift domain distribution that is quite similar to that proposed for the Quseir margin but, again, mantle exhumation, magmatic and continental and oceanic domains in the NRS is far from being proved, and interpretations remain well within the uncertainty of the current modelling from potential field data. A similarity with the model of Karner *et al.* (2021) for the Pelotas/Santos and Campos basins can be determined for what concerns necking and distal domain localization, that correlates to distinct geological processes that dominate and record distinct changes in the geodynamic processes across different domains. In detail there are of course differences, for example the width of the Brazilian South Atlantic margin is significantly greater than that observed for the current NRS (in both the Saudi and Egyptian margins). It is worthy of note that the necking in Egypt within this study places close to the present-day coastline, possibly drawing similarities with the Campos basin. Regarding the nature of the crust basinwards of the necking, observations within this study, and Ali *et al.* (2022b), Ball *et al.* (2018a), Keller *et al.* (2018) and Cochran and Karner (2007), could lead to a conclusion that the hyperextended domain is not amagmatic. This domain could have some similarities with the “continental and magmatic domain” of the Campos basin, but at present within the NRS this region is not directly comparable when exploring the width of the magmatic and continental domains. Further work is needed in the NRS to better determine the amount and age of the magmatics to further classify this domain.

Regarding magmatic evolution, the first-order robust observation is that in the NRS we do not see present day evidence for SDRs, which suggest that, compared to Brazil, fewer magmatic additions reached the surface during rifting, this first-order difference suggests that comparison with Pelotas, southern Santos nor Campos is not required, these margin segments are not similar. The data resolution for Brazil that allows distinct pre-, syn- and post-rift magmatism discussions is not yet available for the NRS within the current analysis. Nevertheless, the role of magmatism in the development of the NRS margin is important,

although it remains poorly defined both spatially and temporally. Early syn-rift magmatism is limited to few direct observations and a few inferred, the latter in particular which need to be further developed, mapped, sampled and dated. In the NRS early syn-rift magmatism is observed, firstly there is evidence that at 25 Ma gabbro underplating occurred within the lower crust. This syn-rift gabbro has been exhumed during rifting at the Brother Islands (Ligi *et al.* 2018). At 23-22 Ma basalts emplaced in numerous dikes (see details in Bosworth *et al.* 2015; Bosworth and Stockli 2016) are found in the Gulf of Suez, in a broad region around Cairo, Egypt, locally onshore Red Sea between Safaga and Quseir, and at Al Wajh and further inland along the Saudi margin (Ott d'Estevou *et al.* 1986; Bosworth *et al.* 1998; Plaziat *et al.* 1998; Bosworth and McClay 2001). Regarding the NRS magmatism, it may be possible to conclude that there are broad similarities between Campos and the NRS in the sense that they both have an early magmatic history and a later post-necking magmatic event. This post-necking magmatic event in the Quseir area, cannot be directly associated, at the moment, with a specific rifting stage (like the post-breakup in Brazil: Karner *et al.* 2021) but rather all we observe is that there is a temporal and a regional change in the magmatic budget of the NRS (Ali *et al.* 2022b). Neither is it clear with the current data that in the NRS that we have enough data to confirm that the rifting has led to the formation of a new coherent plate boundary where continental lithospheric extension is completely broken.

In the framework of the collected data and previous literature, and based on the interpretations of the architecture of the rifted margin at the latitude of Quseir, it is thus possible to propose only a speculative, hypothetical rift evolutionary model. This latter includes three distinct stages:

*Stage 1:* Extension in the NRS was initially accompanied by magmatic intrusions in the lower crust, which led to the emplacement of large gabbroic plutons derived from asthenospheric melts (Fig. 13a; Ligi *et al.* 2018). At the surface, a contemporaneous and generalized stretching phase (cfr. *decoupled tectonics* of Sutra *et al.* 2013) led to the formation of a graben and half-graben net on the whole rift area (i.e., the Egyptian Quseir and the conjugate, namely the Duba zone: Bosworth 2015). Duwi and Hamadat synclines in the Quseir onshore of the Egyptian margin (Fig. 12c) and the Midyan and Azlam basins on the Saudi Arabian side (e.g., Bohannon *et al.* 1989) represent the remnants of these structures (Fig. 12a). Syn-tectonic Late Oligocene sediments (Nakheil Fm.) deposited inside the grabens, unconformably covering the pre-rift Cretaceous-Eocene formations. A significant uplift and erosion phase during the latest Oligocene to Early Miocene (25 to 21 Ma) was proposed (Montenat *et al.* 1988; Omar and Steckler 1995; Bosworth and Burke 2005) to

explain the thin sedimentary units that are preserved inside the grabens and the unconformity with the Pliocene sequence. Nevertheless, it is impossible to assess which kind of sedimentation took place inside the basins, and the Pliocene succession is usually found in unconformity over the entire NRS on top of different sedimentary sequences. Thus, the Late Oligocene succession can be considered an equivalent of the Syn-Tectonic Sequence (STS1) of Decarlis *et al.* (2015), the depositional sequence characteristic of the initial stage of rifting over large areas and showing growth strata (Fig. 12c). Based on the thermochronological data from the onshore Saudi Arabian margin, two widespread exhumation phases are observed and correlated with the development of the Red Sea: the first rift phase was during the Early Miocene at ~23 Ma and the second extensional event was in the Middle Miocene at ~15 Ma (Szymanski *et al.* 2016).

*Stage 2:* During the Early Miocene, tectonics delocalized towards the future axis of rifting. A NE-dipping major detachment fault was initiated at the present-day shoreline, exposing the basement at the surface along the footwall (Fig. 13b). In the more proximal area, upper continental crust and pre-rift and early syn-rift sedimentary covers are dislocated on the detachment as rider blocks, while the seaward, more profound sector of the crust reaches the surface. The new extensional mechanism promoted a thinning of the crust. It formed the distal margin, which was progressively uplifted, leading to the formation of the characteristic along shore, elongated necking basin filled with sediments shed from the onshore area (cfr. thinning phase, coupled tectonics of Sutra *et al.* 2013). Thick Early-Middle Miocene deep marine sediments and evaporites accumulated in this sector forming, together with the clastics as mentioned above, the distal margin sedimentary sequence (cfr. STS2, Decarlis *et al.* 2015). At the end of the Miocene, the evaporite level was below the range of the global sea level (−132 m air-loaded or −192 m water-loaded), suggesting that the Red Sea rifted margin was under-filled and in a shallow water condition where the water level was unstable and decreased during the deposition of the Upper Miocene Zeit Formation (Mitchell *et al.* 2021, 2022). The erosion of the Upper Miocene layered evaporites correlated to an abrupt short-lived drawdown of the Red Sea level during the latest Miocene or the earliest Pliocene (Mitchell *et al.* 2021). The S-reflector is obvious above the salt structures, while, in the embayments and basins, the erosion surface is unclear and the Pliocene sequence is conformable above the layered evaporites suggesting a depositional continuity (Figs. 5-7). This phase of lithospheric extension was accompanied by sparse basaltic volcanism, which is also recorded in the Gulf of Suez and central Red Sea (Stockli and Bosworth 2019). In this stage, the Egyptian

Red Sea margin in Quseir can be interpreted as a lower-plate margin, while the Saudi Arabian margin is identified as an upper-plate (Fig. 13b). It is probably during this stage that exhumation of the lower crust and eventually subcontinental mantle may have occurred in the axial part of the section, as discussed with the 2D forward modelling results.

*Stage 3:* A new deformation phase occurred in the Late Miocene, leading to the development of a new major SW dipping detachment fault. This latter penetrated the lower crust leading to the exhumation of the underplated gabbroic bodies at the surface of the Brothers Islands (Fig. 13c). It is possible that this new detachment fault insists on a previously existing rheologic boundary, for example, between infiltrated and non-infiltrated crust, as postulated in Fig. 10. The formation of a multiple detachment system favors a very advanced stage of hyperextension (e.g., Gillard *et al.* 2015). This extension mode has been observed at present only at this specific location. However, if such continental crust flip-flop detachments are consistently proved elsewhere, they may explain the large amount of extension in the NRS and, eventually, the limited presence of exhumed continental mantle zone. Currently, there is no strong evidence for the structure and nature of the crust in the axial domain of the Quseir offshore, as the available seismic data does not cover the deep zone. Nevertheless, we applied some geologic attributes to a model of different types of crust in the distal sector and compared them with the measured gravity and magnetic anomalies. Our first-order 2D models show that the best fit is obtained with a model including a limited mantle exhumation at the axis. This model was set with a serpentized mantle slab with an average length of 40 km and a thickness of 4 km (Fig. 10c), introducing coherent rock densities and supposing that this section does not generate a strong, organized magnetic signal like in other analogues (Bronner *et al.* 2014). Models implying exhumation of crust and oceanic crust emplacement gave more significant errors. This is the last major phase recognized in the study area, but rifting continued to evolve following different dynamics consistent with the increased left-lateral movement of the Arabian and African plates.

#### *Detachments and flip-flopping*

In general, the interpretation of detachments during the rift evolution is not straightforward and requires high-quality data to understand the dynamic rather than a static interpretation. However, it has been argued in other margins where field data permits, such as in examples preserved in the fold and thrust belts, that detachments are a key component of

rifted margin evolution, for example, Alps (e.g., Manatschal 2004; Masini *et al.* 2012; Decarlis *et al.* 2015), Pyrenees (e.g., Mauffret *et al.* 2001; Jammes *et al.* 2010; Tugend *et al.* 2014, 2015), Afar (e.g., Geoffroy *et al.* 2014), Iberia (e.g., Manatschal 2004; Pérez-Gussinyé 2013; Mohn *et al.* 2015), Australia (e.g., Gillard *et al.* 2015, 2016). Interpretation and analysis of detachment faults lead to the understanding of the lithospheric extension processes of the rifted margins and to the determination of the lower and upper blocks (Lister *et al.* 1986).

The conceptual model presented here is unique in that it describes the evolution of NE and SW-dipping detachments within the Red Sea that allows the crust to thin and exhume lower crust and eventually the mantle in the preferred model scenario. The timing of these detachments is important, and earlier studies had highlighted the observation of detachments exhuming lower crust and mantle to the paleorift surface based on field and seismic data from the Saudi Arabian margin (Ball *et al.* 2018a; Keller *et al.* 2018; Masini *et al.* 2020). Detachments have previously been interpreted in the southern Red Sea in Yemen, where the necking occurred in a magmatic setting, and large granite intrusions were emplaced (e.g., Geoffroy *et al.* 1998). The NE-dipping detachments have been observed in the necked area of the stretched continental crust in the onshore area of the Western Yemen. The thinning of the brittle upper crust induced an upward flexing of the base of the crust and created a rupture zone, where granites were injected passively and sub-vertically (Geoffroy *et al.* 1998). In Eritrea, thick-skinned ductile and thin-skinned brittle regional-scale detachments were observed in the rift shoulder and the Eritrean coastal lowlands. They displace Oligocene lavas and dikes (e.g., Talbot and Ghebreab 1997). The mentioned examples above indicate that the interpreted detachments in the offshore Quseir are much younger than the detachments in the Western Yemen and Eastern Eritrea.

#### *Magmatism, rate of rifting and necking*

Many studies look at the magmatic evolution of the Red Sea (Cochran *et al.* 1986; Coleman and McGuire 1988; Guennoc *et al.* 1988; Martinez and Cochran 1988; Coleman 1993; Cochran 2005; Cochran and Karner 2007; Ali *et al.* 2022a, b). This study documents the occurrence of relatively recent magmatism in the distal margin (Figs. 5, 8 and 14). Therefore, in the Red Sea, early syn-rift magmatism and late-stage magmatism can be identified (Fig. 14). Our observations indicate that stretching, necking, and hyperextension stages are present as well as the existence of recent magmatism in the Quseir sector of the margin (Fig. 14). The onset of rifting is somewhat obscure in the Red Sea, initiation estimates

fall between 33 Ma (Tubbs *et al.* 2014) and 23 Ma (Bosworth *et al.* 2005; Szymanski *et al.* 2016). Ball *et al.* (2018a) and Keller *et al.* (2018) assume that rift initiation is ~23 Ma based on the dating of minor basaltic lavas intruding oldest syn-rift deposits (Fig. 14; Bosworth and Stockli 2016).

Regarding the timing of rifting, we observe that is rapid, occurring only in a few million years. Other studies in the Red Sea that discussed the onset of necking and the role of detachments are Ball *et al.* (2018a), Keller *et al.* (2018) and Masini *et al.* (2020). All indicated that the deposition of the salt layer was simultaneous with the exhumation of the lower crust at ~15-14 Ma along the NRS (Fig. 14). Masini *et al.* (2020) argued this was contemporaneous with the change in the kinematics of the Red Sea linked to the onset of the Dead Sea transform. These earlier studies indicated necking onset between 20-15 Ma (Fig. 14; Ball *et al.* 2018a; Masini *et al.* 2020). In our model, we preferred a scenario in the NRS that invoked exhumation of the lower crust and eventually the mantle, therefore arguing against continuous seafloor spreading in the NRS, our model is therefore in agreement with Ligi *et al.* (2018) and others. This strongly contrasts with the models of Augustin *et al.* (2021) and Tapponnier *et al.* (2013), who respectively argue for breakup ages of 12 Ma and 15 Ma.

## Conclusions

This paper presents a detailed rift domain model interpretation for the NRS. The interpretation of different geophysical and literature databases led to recognizing different rifted margin domains along a section from Quseir to the offshore rift axis zone. In particular, the ***proximal margin domain*** was recognized in the onshore section. It is characterized by a syn-tectonic succession deposited inside well-defined half-graben structures affecting a regular thickness continental crust (30-35 km). The development of the ***necking zone*** due to the hyper-extensional process began probably during the Early Miocene when the crust thinned eastward from 32 km below the Quseir onshore to about 22 km beneath the necking domain. During this stage, the rate of rifting was rapidly occurring only in a few millions of years. The ***distal margin domain*** was reconstructed along the offshore section and is characterized by the deposition of a specific tectonostratigraphic sequence composed principally of evaporites. The thickness of the continental crust thinned from 22 km in the necking zone to less than 10 km below the distal margin.

The observation of the seismo-stratigraphic sequences and their relationships with the

significant faults identified from seismic interpretation, coupled with the existing literature data, allowed the reconstruction of a possible three-stages model for the evolution of rifting in the NRS. **The first stage** accounts for the underplating of magma at the base of the crust and the formation of half-graben basins at the surface, hosting the latest Oligocene/earliest Miocene (25-23 Ma) early rift sequence. **The second stage** consists of a significant thinning of the crust, operated via a significant, east-dipping detachment fault (F1) that led to the progressive exhumation of continental crust basement rocks in the offshore section. Thick Early to Middle Miocene predominantly marine sediments and evaporites accumulated in this sector. The possibility that lower crustal and mantle sections were exhumed during this stage was investigated using 2D forward models. These models indicate the best fit by including a limited mantle exhumation at the axis. The Egyptian margin forms the footwall of the first order detachment faults, and Saudi Arabia represents the hanging wall. **The third stage** developed during the Late Miocene when a prominent west-dipping detachment cut the footwall of the first fault. As a result, lower crustal gabbro was brought to the surface in the Brothers Islands area. This dip polarity switch is probably related to developing a flip-flop detachment system. The third stage of rifting was accompanied by late-stage magmatism during the Pleistocene to Recent, for example, seen on Zabargad Island. This is the last major phase of rifting recognized in the study area, but rifting continued to evolve following different dynamics consistent with the increased left-lateral movement between the Arabian and Sinai plates and resultant oblique opening across the NRS.

The results presented here for the Northern Red Sea are based on the limited data available, and significant aspects of our model will require further investigation. Specifically, future advances would greatly benefit from acquiring state-of-the-art, margin-to-margin reflection seismic lines and making these data available in the public realm.

### **Figures caption**

Fig. 1. Major structural and geological features of the Red Sea (Faults and shear zones, deeps and spreading ridges), the uplifted margins of the Nubian Shield (ANS) and Arabian and the distribution of volcanic islands and Late Cenozoic lava fields (modified from Stern and Johnson 2019). DS and ZFZ indicate the Dead Sea and Zabargad Fracture Zone, respectively.

Fig. 2. Geological and structural map of the Northern Red Sea Region, compiled after Ben-Avraham (1985), Khalil (1998), Hughes *et al.* (2000), Bosworth and McClay (2001), Khalil and McClay (2001, 2009), Ehrhardt *et al.* (2005), Bosworth *et al.* (2017), modified. The red box indicates the study area. CFS and BFS indicate the coastal and the border fault systems, respectively.

Fig. 3. Stratigraphic column of the onshore and offshore Northern Red Sea, from Moustafa and Khalil (2020), Khalil and McClay (2017, 2020) and Bosworth *et al.* (2020), modified.

Fig. 4. (a) Regional map shows the used geophysical data: seismic, gravity and magnetic. The red box represents the "extended discussion area"; the orange polygon indicates the 3D seismic survey. The purple lines indicate 12 ship tracks with both magnetic and gravity surveys between 1958 and 1986. (b) bathymetry map showing the morphology of the study area, the interpreted seismic profiles and the location of the wells used to tie the seismic data.

Fig. 5. (a) Uninterpreted and (b) Interpreted NE-SW composite line-1 (ERS-26 and PRS-72 seismic profiles). The seismic section shows several normal faults (white lines), the thickness variation of the syn-rift sediments, three major salt diapirs and an unconformity surface (S-reflector) between the layered evaporites and Plio-Quaternary sediments. SD indicates salt diapirs.

Fig. 6. (a) Uninterpreted and (b) Interpreted NE-SW crossline 3900. The seismic section illustrates four salt diapirs (SD) and several normal faults (white lines) in the central part of the study area.

Fig. 7. (a) Uninterpreted and (b) Interpreted NE-SW crossline 5000. The seismic profile depicts clearly two salt diapirs (SD) in the northwestern part of the study area, several normal faults (white lines) and a major half-graben structure in the northeastern part of the seismic profile.

Fig. 8. (a) Free-air gravity anomaly map of the central Egyptian Red Sea margin region. (b) RTP anomaly map of the study area. The white star indicates the position of Brothers Islands; the red circle represents the available wells and the blue line represents the track of the forward models.

Fig. 9. 2D forward model in the NE-SW direction crossing the onshore and offshore of the Egyptian Red Sea margin. (a) Observed vs predicted magnetic anomalies and (b) measured vs predicted free-air gravity anomalies. (c) Modelled cross-section including lower crust exhumation and an overlying thick evaporite sequence. Results provide a low match between the measured and predicted gravity and magnetic anomalies across the deeper axial sector of the NRS.

Fig. 10. 2D forward model including mantle exhumation in the distal sector. (a) Observed vs predicted magnetic values and (b) measured vs predicted free-air gravity values. (c) Geological model used for the forward modeling. The good fit between measured and predicted values suggests the possibility of the existence of a mantle exhumation stage in the NRS.

Fig. 11. 2D forward model simulating seafloor spreading initiation at the rift axis. (a) Measured vs predicted magnetic anomaly and (b) observed vs predicted free-air gravity anomaly. (c) The geological cross-section used for the forward modeling. Large discrepancies between measured and predicted gravity and magnetic values are found at the oceanic sector suggesting that the NRS has not reached the stage of seafloor spreading.

Fig. 12. Geological and structural map for the proximal margin west of the Quseir. a) Landsat image showing the main structural elements of the Quseir area in the Egyptian margin and Al Wajh accommodation zone in the Saudi Arabia side. Red lines represent the Miocene normal faults dipping SW, while blue lines indicate the NE-dipping Early Miocene faults. HSZ= Hamrawin shear zone. b) Elevation map showing the main sub-basins in the Quseir onshore, the coastal (CFS) and the border (BFS) fault systems. ZF and AF indicate the Zug El Bahar and Anz segments of the CSF, respectively; HF, NF and KF, represent the Hamadat, Nakheil, and Kallahin segments of the BFS, respectively. DAZ and WEN represent the Duwi accommodation zone

and Wadi El Nakheil, respectively (modified from Khalil and McClay 2002). c) Three cross-sections passing through the Duwi and Hamadat synclines showing the variations of the thickness of the pre-rift and syn-rift sediments and of the dips of the major normal faults and shear zones cutting the proximal domain (upper panels). RTP and gravity anomalies along the displayed cross-sections (lower panels, modified from Khalil and McClay 2002). Location of the three sections is in Figure 12b.

Fig. 13. Proposed evolutionary model for rift stages and onset of mantle exhumation across the Egyptian and Saudi Arabian margins.

Fig. 14. Summary scheme displaying rift phases and the magmatism stages as well as the deposition time of the evaporites in the NRS. Paleo-latitudes from van Hinsbergen *et al.* (2015).

### Tables caption

Table 1. Average density, magnetic susceptibility and seismic velocity of the interpreted seismic units in the NRS (Gettings *et al.* 1986; Bonatti and Seyler 1987; Makris and Rihm 1987; Cochran *et al.* 1991; Saleh *et al.* 2006; Salem *et al.* 2013).

### Acknowledgements

The research was supported by KU project RCII-2019-007 (A. C. and A. D.) and KUIRF Research grants (UAE) project 8474000227-FSU-2020-02 (A. D.). Gridded satellite-derived free-air gravity anomaly data are available from [https://topex.ucsd.edu/pub/global\\_grav\\_1min](https://topex.ucsd.edu/pub/global_grav_1min), the WGM2012 global gravity model (Bouguer anomalies) from <https://bgi.obs-mip.fr/data-products/grids-and-models/wgm2012-global-model/>, and the EMAG2v3 earth magnetic anomaly grid is available from EMAG2<sub>v3</sub>: Earth Magnetic Anomaly Grid (2-arc-minute resolution)-catalog (data.gov). The seismic data were provided courtesy of BG Egypt (now Royal Dutch Shell) and images are published with the permission of South Valley Egyptian Petroleum Holding Company (Ganope). We are grateful to these organizations for providing the data and approval to publish the paper.

### References

Ali, M. 2020. Three-Dimensional Structural Modelling and Source Rock Evaluation of the Quseir Formation in the Komombo Basin, Egypt. *Acta Geologica Sinica -English*

*Edition*, **94**, 1619–1634.

- Ali, M., Darwish, M., Essa, M.A. and Abdelhady, A. 2018. 2D seismic interpretation and characterization of the Hauterivian–Early Barremian source rock in Al Baraka oil field, Komombo Basin, Upper Egypt. *Journal of African Earth Sciences*, **139**, 113–119.
- Ali, M., Abdelmaksoud, A., Essa, M.A., Abdelhady, A. and Darwish, M. 2020. 3D structural, facies and petrophysical modeling of C member of Six Hills Formation, Komombo Basin, Upper Egypt. *Natural Resources Research*, **29**, 2575–2597.
- Ali, M., Ligi, M., Ceriani, A., Bouchaala, F., Bosworth, W. and Decarlis, A. 2022a. Birth of a large Quaternary volcanic edifice southwest of the Brothers Islets, Northern Red Sea, Egyptian Margin. In: *Working Group on Mediterranean Ophiolites Conference, Abstracts*. 1.
- Ali, M., Ligi, M., Ceriani, A., Bouchaala, F., Bosworth, W. and Decarlis, A. 2022b. Geophysical evidence for magmatism southwest of the Brothers Islands, Northern Red Sea (offshore Quseir, Egypt). *Tectonics*, **41**, e2022TC007228.
- Ali, M., Ali, M.Y., Abdelhady, A. and Fairhead, J.D. 2022c. Tectonic evolution and subsidence history of the Cretaceous basins in southern Egypt: the Komombo Basin. *Basin Research*, **34**, 1731–1762.
- Almalki, K.A., Betts, P.G. and Ailleres, L. 2015. The Red Sea–50 years of geological and geophysical research. *Earth-Science Reviews*, **147**, 109–140.
- ArRajehi, A., McClusky, S., et al. 2010. Geodetic constraints on present-day motion of the Arabian Plate: Implications for Red Sea and Gulf of Aden rifting. *Tectonics*, **29**.
- Augustin, N., Van der Zwan, F.M., Devey, C.W. and Brandsdóttir, B. 2021. 13 million years of seafloor spreading throughout the Red Sea Basin. *Nature Communications*, **12**, 1–10.
- Ball, P., Ion, D., Salem, A., Keller, J. and Borsato, R. 2018a. Rift models for the central segment of the Northern Red Sea. In: *EGU General Assembly Conference Abstracts*. 11950.
- Ball, P.J., Stockli, D.F., Robbins, S., Tugend, J. and Masini, E. 2018b. Northern Red Sea: Unravelling the tectono-thermal evolution of a hyper-extended rift system. *La Réunion des Sciences de la Terre, Abstract*, 245.
- Balmino, G., Vales, N., Bonvalot, S. and Briais, A. 2012. Spherical harmonic modelling to ultra-high degree of Bouguer and isostatic anomalies. *Journal of Geodesy*, **86**, 499–520.
- Barakat, H. and Miller, P. 1984. Geology and petroleum exploration, Safaga concession, northern Red Sea, Egypt. In: *Proceedings of the 7th Exploration Seminar, Egyptian General Petroleum Corporation, Cairo*. 191–214.

- Ben-Avraham, Z. 1985. Structural framework of the gulf of Elat (Aqaba), northern Red Sea. *Journal of Geophysical Research: Solid Earth*, **90**, 703–726.
- Bohannon, R.G., Naeser, C.W., Schmidt, D.L. and Zimmermann, R.A. 1989. The timing of uplift, volcanism, and rifting peripheral to the Red Sea: a case for passive rifting? *Journal of Geophysical Research: Solid Earth*, **94**, 1683–1701.
- Bonatti, E. 1985. Punctiform initiation of seafloor spreading in the Red Sea during transition from a continental to an oceanic rift. *Nature*, **316**, 33–37.
- Bonatti, E. and Seyler, M. 1987. Crustal underplating and evolution in the Red Sea rift: uplifted gabbro/gneiss crustal complexes on Zabargad and Brothers Islands. *Journal of Geophysical Research: Solid Earth*, **92**, 12803–12821.
- Bonatti, E., Ottonello, G. and Hamlyn, P.R. 1986. Peridotites from the island of Zabargad (St. John), Red Sea: petrology and geochemistry. *Journal of Geophysical Research: Solid Earth*, **91**, 599–631.
- Bonvalot, S., Balmino, G., et al. 2012. World gravity map. *Commission for the Geological Map of the World*.
- Bosworth, W. 1994. A model for the three-dimensional evolution of continental rift basins, north-east Africa. *Geologische Rundschau*, **83**, 671–688.
- Bosworth, W. 2015. Geological evolution of the Red Sea: historical background, review, and synthesis. *In: The Red Sea*. 45–78.
- Bosworth, W. and Burke, K. 2005. Evolution of the Red Sea—Gulf of Aden rift system. *Petroleum systems of divergent continental margin basins*, 342–372.
- Bosworth, W. and McClay, K. 2001. Structural and stratigraphic evolution of the Gulf of Suez rift, Egypt: a synthesis. *Mémoires du Muséum national d'histoire naturelle (1993)*, **186**, 567–606.
- Bosworth, W. and Stockli, D.F. 2016. Early magmatism in the greater Red Sea rift: timing and significance. *Canadian Journal of Earth Sciences*, **53**, 1158–1176.
- Bosworth, W., Sultan, M., Stern, R.J., Arvidson, R.E., Shore, P. and Becker, R. 1993. Nature of the Red Sea crust: A controversy revisited: Comment and Reply. *Geology*, **21**, 574–576.
- Bosworth, W., Crevello, P., Winn, R.D. and Steinmetz, J. 1998. Structure, sedimentation, and basin dynamics during rifting of the Gulf of Suez and north-western Red Sea. *In: Sedimentation and Tectonics in Rift Basins Red Sea:-Gulf of Aden*. 77–96.
- Bosworth, W., Huchon, P. and McClay, K. 2005. The red sea and gulf of aden basins. *Journal of African Earth Sciences*, **43**, 334–378.

- Bosworth, W., Stockli, D.F. and Helgeson, D.E. 2015. Integrated outcrop, 3D seismic, and geochronologic interpretation of Red Sea dike-related deformation in the Western Desert, Egypt—the role of the 23 Ma Cairo “mini-plume”. *Journal of African Earth Sciences*, **109**, 107–119.
- Bosworth, W., Montagna, P., Pons-Branchu, E., Rasul, N. and Taviani, M. 2017. Seismic hazards implications of uplifted Pleistocene coral terraces in the Gulf of Aqaba. *Scientific reports*, **7**, 1–13.
- Bosworth, W., Khalil, S.M., Ligi, M., Stockli, D.F. and McClay, K.R. 2020. Geology of Egypt: The Northern Red Sea. In: *The Geology of Egypt*. 343–374.
- Bronner, A., Sauter, D., Munschy, M., Carlut, J., Searle, R., Cannat, M. and Manatschal, G. 2014. Magnetic signature of large exhumed mantle domains of the Southwest Indian Ridge—results from a deep-tow geophysical survey over 0 to 11 Ma old seafloor. *Solid Earth*, **5**, 339–354.
- Capitanio, F.A., Nebel, O. and Cawood, P.A. 2020. Thermochemical lithosphere differentiation and the origin of cratonic mantle. *Nature*, **588**, 89–94.
- Chenin, P., Manatschal, G., Lavier, L.L. and Erratt, D. 2015. Assessing the impact of orogenic inheritance on the architecture, timing and magmatic budget of the North Atlantic rift system: a mapping approach. *Journal of the Geological Society*, **172**, 711–720.
- Chenin, P., Schmalholz, S.M., Manatschal, G. and Duretz, T. 2020. Impact of crust–mantle mechanical coupling on the topographic and thermal evolutions during the necking phase of ‘magma-poor’ and ‘sediment-starved’ rift systems: A numerical modeling study. *Tectonophysics*, **786**, 228472.
- Cochran, J.R. 1983. A model for development of Red Sea. *Aapg Bulletin*, **67**, 41–69.
- Cochran, J.R. 2005. Northern Red Sea: Nucleation of an oceanic spreading center within a continental rift. *Geochemistry, Geophysics, Geosystems*, **6**.
- Cochran, J.R. and Karner, G.D. 2007. Constraints on the deformation and rupturing of continental lithosphere of the Red Sea: the transition from rifting to drifting. *Geological Society, London, Special Publications*, **282**, 265–289.
- Cochran, J.R., Martinez, F., Steckler, M.S. and Hobart, M.A. 1986. Conrad Deep: a new northern Red Sea deep: origin and implications for continental rifting. *Earth and Planetary Science Letters*, **78**, 18–32.
- Cochran, J.R., Gaulier, J. and Le Pichon, X. 1991. Crustal structure and the mechanism of extension in the northern Red Sea: Constraints from gravity anomalies. *Tectonics*, **10**,

1018–1037.

- Coleman, R.G. 1993. Geological evolution of the Red Sea. *Oxford Monographs on Geology and Geophysics*. Oxford University Press, New York, **24**, 186.
- Coleman, R.G. and McGuire, A.V. 1988. Magma systems related to the Red Sea opening. *Tectonophysics*, **150**, 77–100.
- Cooper, G.R.J. and Cowan, D.R. 2005. Differential reduction to the pole. *Computers & Geosciences*, **31**, 989–999.
- Decarlis, A., Manatschal, G., Hauptert, I. and Masini, E. 2015. The tectono-stratigraphic evolution of distal, hyper-extended magma-poor conjugate rifted margins: Examples from the Alpine Tethys and Newfoundland–Iberia. *Marine and Petroleum Geology*, **68**, 54–72.
- Decarlis, A., Fellin, M.G., et al. 2017. Tectono-thermal Evolution of a Distal Rifted Margin: Constraints From the Calizzano Massif (Prepiedmont-Briançonnais Domain, Ligurian Alps). *Tectonics*, **36**, 3209–3228.
- Duncan, R.A. and Al-Amri, A.M. 2013. Timing and composition of volcanic activity at Harrat Lunayyir, western Saudi Arabia. *Journal of Volcanology and Geothermal Research*, **260**, 103–116.
- Duret, T., Asti, R., Lagabrielle, Y., Brun, J., Jourdon, A., Clerc, C. and Corre, B. 2020. Numerical modelling of Cretaceous Pyrenean Rifting: The interaction between mantle exhumation and syn-rift salt tectonics. *Basin Research*, **32**, 652–667.
- Ehrhardt, A., Hübscher, C., Ben-Avraham, Z. and Gajewski, D. 2005. Seismic study of pull-apart-induced sedimentation and deformation in the Northern Gulf of Aqaba (Elat). *Tectonophysics*, **396**, 59–79.
- El Khrepy, S., Koulakov, I., Gerya, T., Al-Arifi, N., Alajmi, M.S. and Qadrouh, A.N. 2021. Transition from continental rifting to oceanic spreading in the northern Red Sea area. *Scientific Reports*, **11**, 1–7.
- Gaulier, J.M., Le Pichon, X., et al. 1988. Seismic study of the crust of the northern Red Sea and Gulf of Suez. *Tectonophysics*, **153**, 55–88.
- Geoffroy, L., Huchon, P. and Khanbari, K. 1998. Did Yemeni Tertiary granites intrude neck zones of a stretched continental upper crust? *Terra Nova*, **10**, 196–200.
- Geoffroy, L., Le Gall, B., Daoud, M.A. and Jalludin, M. 2014. Flip-flop detachment tectonics at nascent passive margins in SE Afar. *Journal of the Geological Society*, **171**, 689–694.
- Gettings, M.E., Blank Jr, H.R., Mooney, W.D. and Healey, J.H. 1986. Crustal structure of southwestern Saudi Arabia. *Journal of Geophysical Research: Solid Earth*, **91**, 6491–

6512.

- Gillard, M., Autin, J., Manatschal, G., Sauter, D., Munsch, M. and Schaming, M. 2015. Tectonomagmatic evolution of the final stages of rifting along the deep conjugate Australian-Antarctic magma-poor rifted margins: Constraints from seismic observations. *Tectonics*, **34**, 753–783.
- Gillard, M., Autin, J. and Manatschal, G. 2016. Fault systems at hyper-extended rifted margins and embryonic oceanic crust: Structural style, evolution and relation to magma. *Marine and Petroleum Geology*, **76**, 51–67.
- Girdler, R.W. 1990. The Dead Sea transform fault system. *Tectonophysics*, **180**, 1–13.
- Girdler, R.W. and Underwood, M. 1985. The evolution of early oceanic lithosphere in the southern Red Sea. *Tectonophysics*, **116**, 95–108.
- Girdler, R.W. and Whitmarsh, R. 1974. Miocene Evaporites in Red Sea cores, their relevance to the problem of the width and age of oceanic crust beneath the Red Sea.
- Gordon, G., Hansen, B., et al. 2010. The hydrocarbon prospectivity of the Egyptian North Red Sea basin. *In: Geological Society, London, Petroleum Geology Conference Series*. 783–789.
- Guennoc, P., Pautot, G. and Coutelle, A. 1988. Surficial structures of the northern Red Sea axial valley from 23 N to 28 N: time and space evolution of neo-oceanic structures. *Tectonophysics*, **153**, 1–23.
- Haupt, I., Manatschal, G., Decarli, A. and Unternehr, P. 2016. Upper-plate magma-poor rifted margins: Stratigraphic architecture and structural evolution. *Marine and Petroleum Geology*, **69**, 241–261.
- Hosny, A. and Nyblade, A. 2014. Crustal structure in southeastern Egypt: Symmetric thinning of the northern Red Sea rifted margins. *Geology*, **42**, 219–222.
- Hosny, A. and Nyblade, A. 2016. The crustal structure of Egypt and the northern Red Sea region. *Tectonophysics*, **687**, 257–267.
- Hughes, G.W. and Beydoun, Z.R. 1992. The Red Sea—Gulf of Aden: biostratigraphy, lithostratigraphy and palaeoenvironments. *Journal of Petroleum Geology*, **15**, 135–156.
- Hughes, G.W., Perincek, D., Abu-Bshait, A.-J. and Jarad, A.-R.M. 2000. Aspects of Midyan geology, Saudi Arabian Red Sea. *Saudi Aramco Journal of Technology*, **1999**, 12–42.
- Hughes, G.W. ap G. and Johnson, R.S. 2005. Lithostratigraphy of the Red Sea region. *GeoArabia*, **10**, 49–126.
- Incerpi, N., Martire, L., et al. 2020. Hydrothermal fluid flow associated to the extensional evolution of the Adriatic rifted margin: Insights from the pre- to post-rift sedimentary

- sequence (SE Switzerland, N ITALY). *Basin Research*, **32**, 91–115.
- Jagoutz, O., Muntener, O., Manatschal, G., Rubatto, D., Péron-Pinvidic, G., Turrin, B.D. and Villa, I.M. 2007. The rift-to-drift transition in the North Atlantic: A stuttering start of the MORB machine? *Geology*, **35**, 1087–1090.
- Jammes, S., Tiberi, C. and Manatschal, G. 2010. 3D architecture of a complex transcurrent rift system: The example of the Bay of Biscay–Western Pyrenees. *Tectonophysics*, **489**, 210–226.
- Jarrige, J., Ott d'Estevou, P., Burolet, P.F., Montenat, C., Prat, P., Richert, J. and Thiriet, J. 1990. The multistage tectonic evolution of the Gulf of Suez and northern Red Sea continental rift from field observations. *Tectonics*, **9**, 441–465.
- Joffe, S. and Garfunkel, Z. 1987. Plate kinematics of the circum Red Sea—a re-evaluation. *Tectonophysics*, **141**, 5–22.
- Karner, G.D. 2000. AAPG Memoir 73, Chapter 21: Rifts of the Campos and Santos Basins, Southeastern Brazil: Distribution and Timing.
- Karner, G.D., Johnson, C., et al. 2021. Tectono-magmatic development of the Santos and Campos basins, offshore Brazil. In: *The Supergiant Lower Cretaceous Presalt Petroleum Systems of the Santos Basin*. 124: 215-256.
- Keating, P. and Zerbo, L. 1996. An improved technique for reduction to the pole at low latitudes. *Geophysics*, **61**, 131–137.
- Keller, J., Ion, D., Salem, A. and Ball, P. 2018. Rift architecture and evolution of the Northern Red Sea. In: *Conjugate Margins Conference, Halifax, Nova Scotia*.
- Khalil, S.M. 1998. Tectonic evolution of the eastern margin of the Gulf of Suez, Egypt.
- Khalil, S.M. and McClay, K.R. 2001. Tectonic evolution of the NW Red Sea-Gulf of Suez rift system. *Geological Society, London, Special Publications*, **187**, 453–473.
- Khalil, S.M. and McClay, K.R. 2002. Extensional fault-related folding, northwestern Red Sea, Egypt. *Journal of Structural Geology*, **24**, 743–762.
- Khalil, S.M. and McClay, K.R. 2009. Structural control on syn-rift sedimentation, northwestern Red Sea margin, Egypt. *Marine and Petroleum Geology*, **26**, 1018–1034.
- Khalil, S.M. and McClay, K.R. 2017. 3D geometry and kinematic evolution of extensional fault-related folds, NW Red Sea, Egypt. *Geological Society, London, Special Publications*, **439**, 109–130.
- Khalil, S.M. and McClay, K.R. 2020. Extensional fault-related folding in the northwestern Red Sea, Egypt: segmented fault growth, fault linkages, corner folds and basin evolution. *Geological Society, London, Special Publications*, **476**, 49–81.

- Lavier, L.L., Ball, P.J., Manatschal, G., Heumann, M.J., MacDonald, J., Matt, V.J. and Schneider, C. 2019. Controls on the Thermomechanical Evolution of Hyperextended Lithosphere at Magma-Poor Rifted Margins: The Example of Espirito Santo and the Kwanza Basins. *Geochemistry, Geophysics, Geosystems*, **20**, 5148–5176.
- Le Magoarou, C., Hirsch, K., Fleury, C., Martin, R., Ramirez-Bernal, J. and Ball, P. 2021. Integration of gravity, magnetic, and seismic data for subsalt modeling in the Northern Red Sea. *Interpretation*, **9**, T507–T521.
- Li, F., Sun, Z., et al. 2021. Compression-induced anomalous subsidence in the extensional sedimentary basin: A numerical study from the Pearl River Mouth Basin, northern South China Sea margin. *Geophysical Research Letters*, **48**, e2021GL094750.
- Li, X. 2008. Magnetic reduction-to-the-pole at low latitudes: Observations and considerations. *The leading edge*, **27**, 990–1002.
- Ligi, M., Bonatti, E., et al. 2011. Initial burst of oceanic crust accretion in the Red Sea due to edge-driven mantle convection. *Geology*, **39**, 1019–1022.
- Ligi, M., Bonatti, E., et al. 2012. Birth of an ocean in the Red Sea: initial pangs. *Geochemistry, Geophysics, Geosystems*, **13**.
- Ligi, M., Bonatti, E., et al. 2018. Birth of an ocean in the Red Sea: Oceanic-type basaltic melt intrusions precede continental rapture. *Gondwana Research*, **54**, 150–160.
- Lister, G.S., Etheridge, M.A. and Symonds, P.A. 1986. Detachment faulting and the evolution of passive continental margins. *Geology*, **14**, 246–250.
- Lyberis, N. 1988. Tectonic evolution of the Gulf of Suez and the Gulf of Aqaba. *Tectonophysics*, **153**, 209–220.
- Mahsoub, M., Abulnasr, R., Boukhary, M., Faris, M. and Abd El Aal, M. 2012. Bio-and sequence stratigraphy of upper cretaceous–palaeogene rocks, east Bahariya concession, Western Desert, Egypt. *Geologia Croatica*, **65**, 109–138.
- Makris, J. and Rihm, R. 1987. Crustal structure of the Red Sea region derived from seismic and gravity data. *Terra Cognita*, **7**, 294.
- Manatschal, G. 2004. New models for evolution of magma-poor rifted margins based on a review of data and concepts from West Iberia and the Alps. *International Journal of Earth Sciences*, **93**, 432–466.
- Manatschal, G., Lavier, L. and Chenin, P. 2015. The role of inheritance in structuring hyperextended rift systems: Some considerations based on observations and numerical modeling. *Gondwana Research*, **27**, 140–164.
- Martinez, F. and Cochran, J.R. 1988. Structure and tectonics of the northern Red Sea:

- catching a continental margin between rifting and drifting. *Tectonophysics*, **150**, 1–31.
- Martinez, F., Muñoz, B., López, C., González, R., Parra, M. and Riquelme, R. 2021. Complex basement-involved contractional structures in the Pre-Andean basins of northern Chile: A review from seismic data. *Tectonics*, **40**, e2020TC006433.
- Masini, E., Manatschal, G., Mohn, G. and Unternehr, P. 2012. Anatomy and tectono-sedimentary evolution of a rift-related detachment system: The example of the Err detachment (central Alps, SE Switzerland). *Bulletin*, **124**, 1535–1551.
- Masini, E., Manatschal, G. and Mohn, G. 2013. The Alpine Tethys rifted margins: Reconciling old and new ideas to understand the stratigraphic architecture of magma-poor rifted margins. *Sedimentology*, **60**, 174–196.
- Masini, E., Stockli, D., Gómez-Romeu, J., Ball, P., Kusznir, N.J. and Calassou, S. 2020. Exploration challenges and perspectives of hyper-extended rift systems: A Northern Red Sea viewpoint. In: *AAPG Middle East Region Geoscience Technology Workshop, Rift Basin Evolution and Exploration*.
- Mauffret, A., de Grossouvre, B.D., Dos Reis, A.T., Gorini, C. and Nercessian, A. 2001. Structural geometry in the eastern Pyrenees and western Gulf of Lion (Western Mediterranean). *Journal of Structural Geology*, **23**, 1701–1726.
- Meyer, B., Saltus, R. and Chulliat, A. 2017. EMAG2 Version 3-Update of a two arc-minute global magnetic anomaly grid. In: *EGU General Assembly Conference Abstracts*. 10614.
- Miller, P.M. and Barakat, H. 1988. Geology of the safaga concession, northern Red Sea, Egypt. *Tectonophysics*, **153**, 123–136.
- Mitchell, N.C. and Park, Y. 2014. Nature of crust in the central Red Sea. *Tectonophysics*, **628**, 123–139.
- Mitchell, N.C., Ligi, M., Ferrante, V., Bonatti, E. and Rutter, E. 2010. Submarine salt flows in the central Red Sea. *Bulletin*, **122**, 701–713.
- Mitchell, N.C., Ligi, M., Feldens, P. and Hübscher, C. 2017. Deformation of a young salt giant: regional topography of the Red Sea Miocene evaporites. *Basin Research*, **29**, 352–369.
- Mitchell, N.C., Ligi, M. and Rasul, N.M.A. 2019. Variations in Plio-Pleistocene Deposition in the Red Sea. In: *Geological Setting, Palaeoenvironment and Archaeology of the Red Sea*. 323–339.
- Mitchell, N.C., Shi, W., Izzeldin, A.Y. and Stewart, I.C.F. 2021. Reconstructing the level of the central Red Sea evaporites at the end of the Miocene. *Basin Research*, **33**, 1266–1292.

- Mitchell, N.C., Hernandez, K., Preine, J., Ligi, M., Augustin, N., Izzeldin, A. and Hübscher, C. 2022. Early stage diapirism in the Red Sea deep-water evaporites: Origins and length-scales. *Tectonophysics*, **831**, 229331.
- Mohn, G., Manatschal, G., Beltrando, M., Masini, E. and Kuszniir, N. 2012. Necking of continental crust in magma-poor rifted margins: Evidence from the fossil Alpine Tethys margins. *Tectonics*, **31**.
- Mohn, G., Karner, G.D., Manatschal, G. and Johnson, C.A. 2015. Structural and stratigraphic evolution of the Iberia–Newfoundland hyper-extended rifted margin: a quantitative modelling approach. *Geological Society, London, Special Publications*, **413**, 53–89.
- Montenat, C., D’Estevou, P.O., et al. 1988. Tectonic and sedimentary evolution of the Gulf of Suez and the northwestern Red Sea. *Tectonophysics*, **153**, 161–177.
- Mooney, W.D., Gettings, M.E., Blank, H.R. and Healy, J.H. 1985. Saudi Arabian seismic-refraction profile: a travelttime interpretation of crustal and upper mantle structure. *Tectonophysics*, **111**, 173–246.
- Moustafa, A.R. 1997. Controls on the development and evolution of transfer zones: the influence of basement structure and sedimentary thickness in the Suez rift and Red Sea. *Journal of Structural Geology*, **19**, 755–768.
- Moustafa, A.R. and Khalil, S.M. 2020. Structural Setting and Tectonic Evolution of the Gulf of Suez, NW Red Sea and Gulf of Aqaba Rift Systems. *In: The Geology of Egypt*. 295–342.
- Omar, G.I. and Steckler, M.S. 1995. Fission track evidence on the initial rifting of the Red Sea: two pulses, no propagation. *Science*, **270**, 1341–1344.
- Ott d’Estevou, P., Bolze, J. and Montenat, C. 1986. Etude géologique de la marge occidentale du Golfe de Suez: le Massif des Gharamul et le Gebel Dara. *Documents et Travaux, Institut Géologique Albert de Lapparent*, **10**, 19–44.
- Patton, T.L., Moustafa, A.R., Nelson, R.A. and Abdine, S.A. 1994. Tectonic evolution and structural setting of the Suez Rift: Chapter 1: Part I. Type Basin: Gulf of Suez.
- Pérez-Gussinyé, M. 2013. A tectonic model for hyperextension at magma-poor rifted margins: an example from the West Iberia–Newfoundland conjugate margins. *Geological Society, London, Special Publications*, **369**, 403–427.
- Pérez-Gussinyé, M., Andrés-Martínez, M., Araújo, M., Xin, Y., Armitage, J. and Morgan, J.P. 2020. Lithospheric strength and rift migration controls on synrift stratigraphy and breakup unconformities at rifted margins: Examples from numerical models, the Atlantic and South China Sea Margins. *Tectonics*, **39**, e2020TC006255.

- Picazo, S., Müntener, O., Manatschal, G., Bauville, A., Karner, G. and Johnson, C. 2016. Mapping the nature of mantle domains in Western and Central Europe based on clinopyroxene and spinel chemistry: Evidence for mantle modification during an extensional cycle. *Lithos*, **266**, 233–263.
- Pinto, V.H.G., Manatschal, G. and Karpoff, A.-M. 2014. Linking the tectonic evolution with fluid history in magma-poor rifted margins: tracking mantle-and continental crust-related fluids. *In: AGU Fall Meeting Abstracts*. OS24A-08.
- Plaziat, J.-C., Baltzer, F., et al. 1998. Quaternary marine and continental sedimentation in the northern Red Sea and Gulf of Suez (Egyptian coast): influences of rift tectonics, climatic changes and sea-level fluctuations. *In: Sedimentation and Tectonics in Rift Basins Red Sea:-Gulf of Aden*. 537–573.
- Quennell, A.M. 1951. *The Geology and Mineral Resources of (Former) Trans-Jordan*.
- Quennell, A.M. 1958. The structural and geomorphic evolution of the Dead Sea Rift. *Quarterly Journal of the Geological Society*, **114**, 1–24.
- Reilinger, R., McClusky, S. and ArRajehi, A. 2015. Geodetic constraints on the geodynamic evolution of the Red Sea. *In: The Red Sea*. 135–149.
- Ribes, C., Ghienne, J.-F., et al. 2020. The Grès Singuliers of the Mont Blanc region (France and Switzerland): stratigraphic response to rifting and crustal necking in the Alpine Tethys. *International Journal of Earth Sciences*, **109**, 2325–2352.
- Ross, D.A. and Schlee, J. 1973. Shallow structure and geologic development of the southern Red Sea. *Geological Society of America Bulletin*, **84**, 3827–3848.
- Saleh, S., Jahr, T., Jentzsch, G., Saleh, A. and Abou Ashour, N.M. 2006. Crustal evaluation of the northern Red Sea rift and Gulf of Suez, Egypt from geophysical data: 3-dimensional modeling. *Journal of African Earth Sciences*, **45**, 257–278.
- Salem, A., Green, C., Campbell, S., Fairhead, J.D., Cascone, L. and Moorhead, L. 2013. Moho depth and sediment thickness estimation beneath the Red Sea derived from satellite and terrestrial gravity data. *Geophysics*, **78**, G89–G101.
- Sandwell, D.T., Müller, R.D., Smith, W.H.F., Garcia, E. and Francis, R. 2014. New global marine gravity model from CryoSat-2 and Jason-1 reveals buried tectonic structure. *Science*, **346**, 65–67.
- Sinadinovski, C., Aldamegh, K., et al. 2017. Passive Seismic Experiment to understand the basement and crustal structure, Northern Red Sea. *EGUGA*, 5986.
- Stern, R.J. and Johnson, P.R. 2019. Constraining the opening of the Red Sea: Evidence from the Neoproterozoic margins and Cenozoic magmatism for a volcanic rifted margin. *In:*

*Geological Setting, Palaeoenvironment and Archaeology of the Red Sea*. 53–79.

- Stockli, D.F. and Bosworth, W. 2019. Timing of extensional faulting along the magma-poor central and northern Red Sea rift margin—transition from regional extension to necking along a hyperextended rifted margin. *In: Geological Setting, Palaeoenvironment and Archaeology of the Red Sea*. 81–111.
- Sutra, E. and Manatschal, G. 2012. How does the continental crust thin in a hyperextended rifted margin? Insights from the Iberia margin. *Geology*, **40**, 139–142.
- Sutra, E., Manatschal, G., Mohn, G. and Unternehr, P. 2013. Quantification and restoration of extensional deformation along the Western Iberia and Newfoundland rifted margins. *Geochemistry, Geophysics, Geosystems*, **14**, 2575–2597.
- Szymanski, E., Stockli, D.F., Johnson, P.R. and Hager, C. 2016. Thermochronometric evidence for diffuse extension and two-phase rifting within the Central Arabian Margin of the Red Sea Rift. *Tectonics*, **35**, 2863–2895.
- Talbot, C.J. and Ghebreab, W. 1997. Red Sea detachment and basement core complexes in Eritrea. *Geology*, **25**, 655–658.
- Taponnier, P., Dymant, J., et al. 2013. Revisiting seafloor-spreading in the Red Sea: basement nature, transforms and ocean-continent boundary. *In: AGU Fall Meeting Abstracts*. T12B-04.
- Tang, Z., Julià, J., Zahran, H. and Mai, P.M. 2016. The lithospheric shear-wave velocity structure of Saudi Arabia: Young volcanism in an old shield. *Tectonophysics*, **680**, 8–27.
- Tewfik, N. and Ayyad, M. 1982. Petroleum exploration in the Red Sea shelf of Egypt. *In: Proc. 6th Exploration Seminar, Egyptian General Petroleum Corporation and Egypt Petroleum Exploration Society, Cairo*. 159–180.
- Tubbs, R.E., Fouda, H.G.A., Afifi, A.M., Raterman, N.S., Hughes, G.W. and Fadolkarem, Y.K. 2014. Midyan Peninsula, northern Red Sea, Saudi Arabia: seismic imaging and regional interpretation. *GeoArabia*, **19**, 165–184.
- Tugend, J., Manatschal, G., Kusznir, N.J., Masini, E., Mohn, G. and Thion, I. 2014. Formation and deformation of hyperextended rift systems: Insights from rift domain mapping in the Bay of Biscay-Pyrenees. *Tectonics*, **33**, 1239–1276.
- Tugend, J., Manatschal, G., Kusznir, N.J. and Masini, E. 2015. Characterizing and identifying structural domains at rifted continental margins: application to the Bay of Biscay margins and its Western Pyrenean fossil remnants. *Geological Society, London, Special Publications*, **413**, 171–203.
- van Hinsbergen, D.J.J., De Groot, L. V., et al. 2015. A paleolatitude calculator for

- paleoclimate studies. *PloS one*, **10**, e0126946.
- Voggenreiter, W., Hötzl, H. and Mechie, J. 1988. Low-angle detachment origin for the Red Sea Rift System? *Tectonophysics*, **150**, 51–75.
- Wernicke, B. 1981. Low-angle normal faults in the Basin and Range Province: nappe tectonics in an extending orogen. *Nature*, **291**, 645–648.
- Younes, A.I. and McClay, K. 2002. Development of accommodation zones in the Gulf of Suez-Red Sea rift, Egypt. *AAPG bulletin*, **86**, 1003–1026.
- Zalán, P.V. 2017. Five kilometers of Paleozoic sediments beneath the pre-salt of Santos basin. *In: International Conference and Exhibition, Barcelona, Spain, 3-6 April 2016*. 29.

ACCEPTED MANUSCRIPT

Figure 1

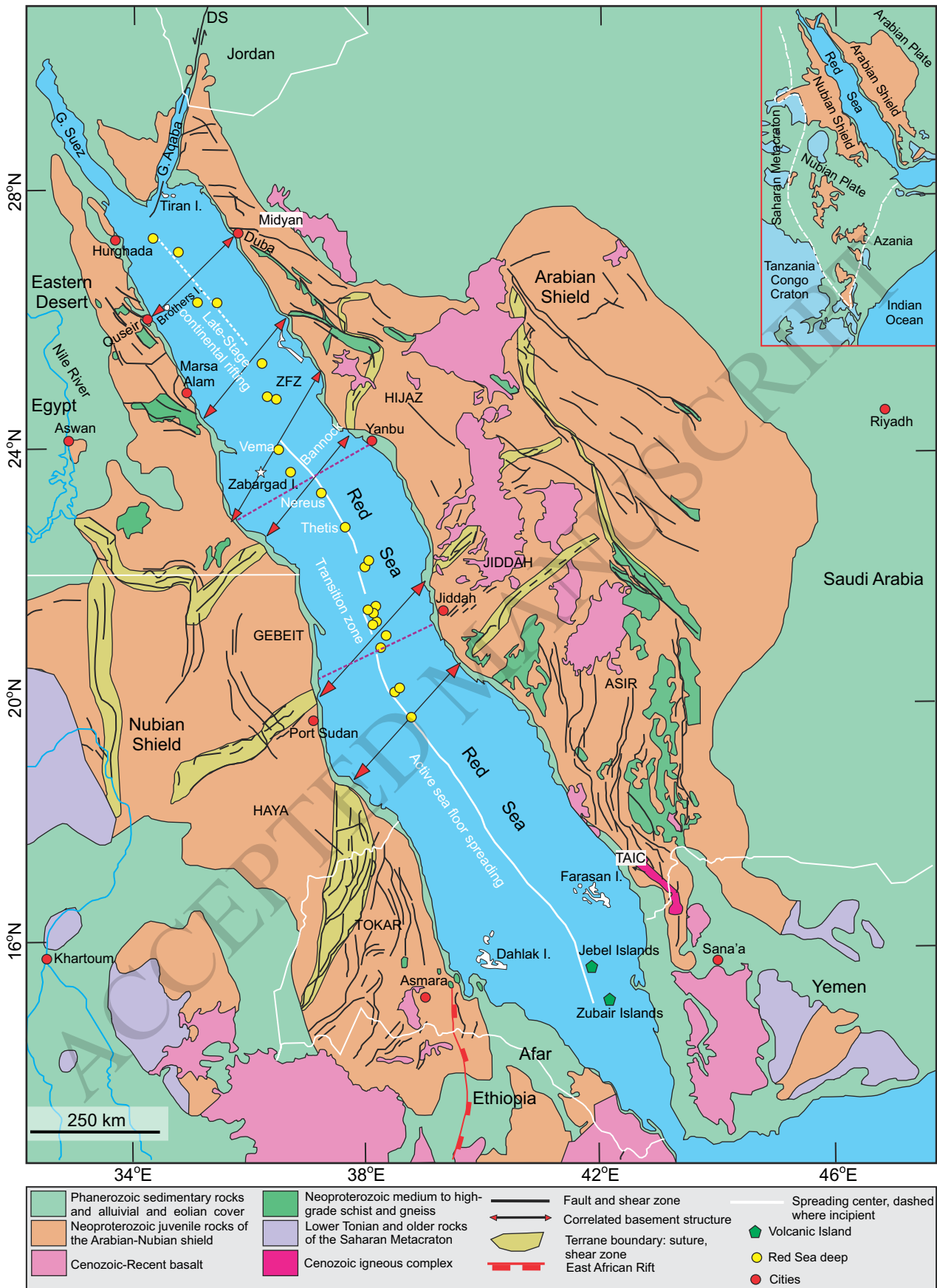


Figure 2

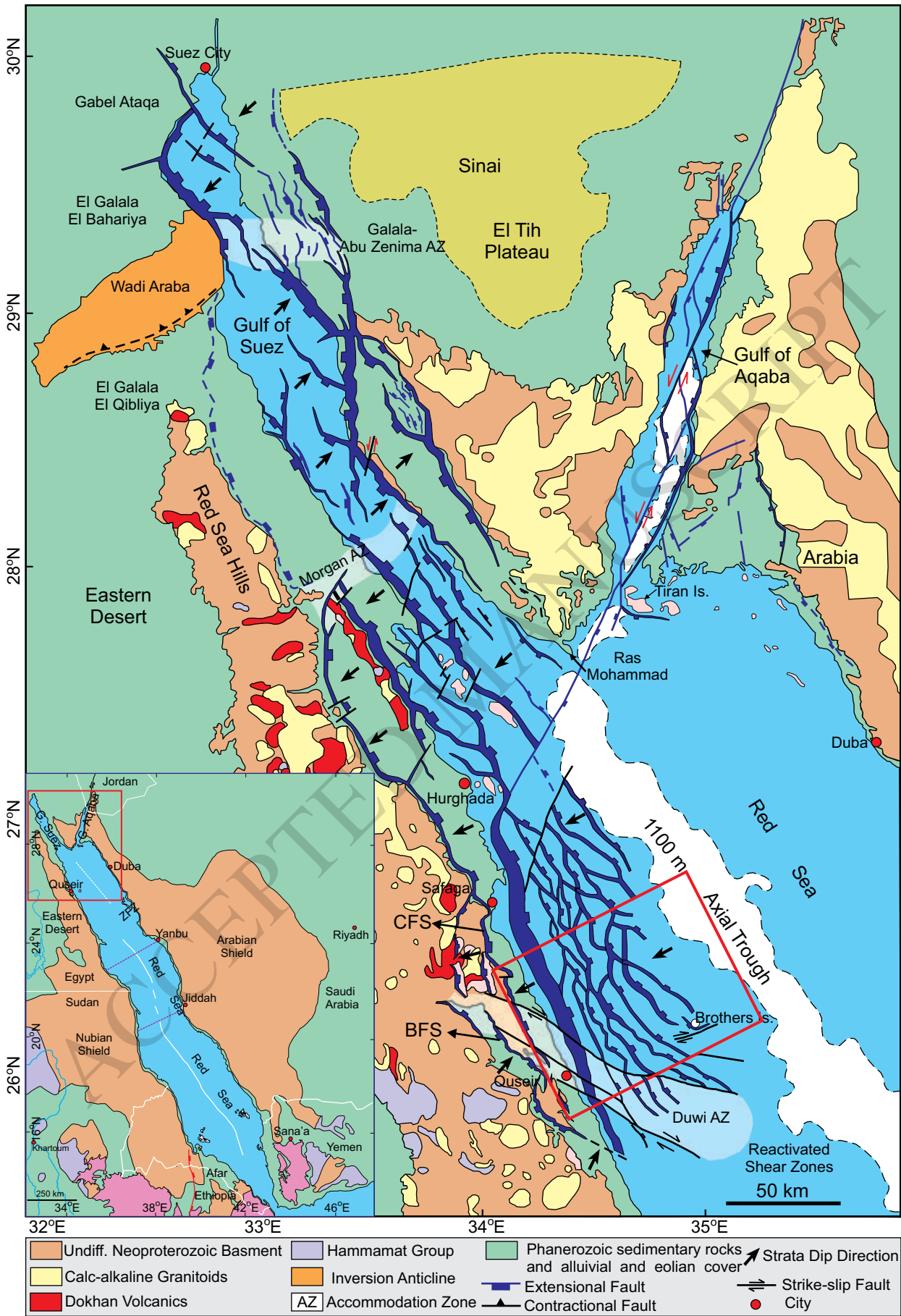
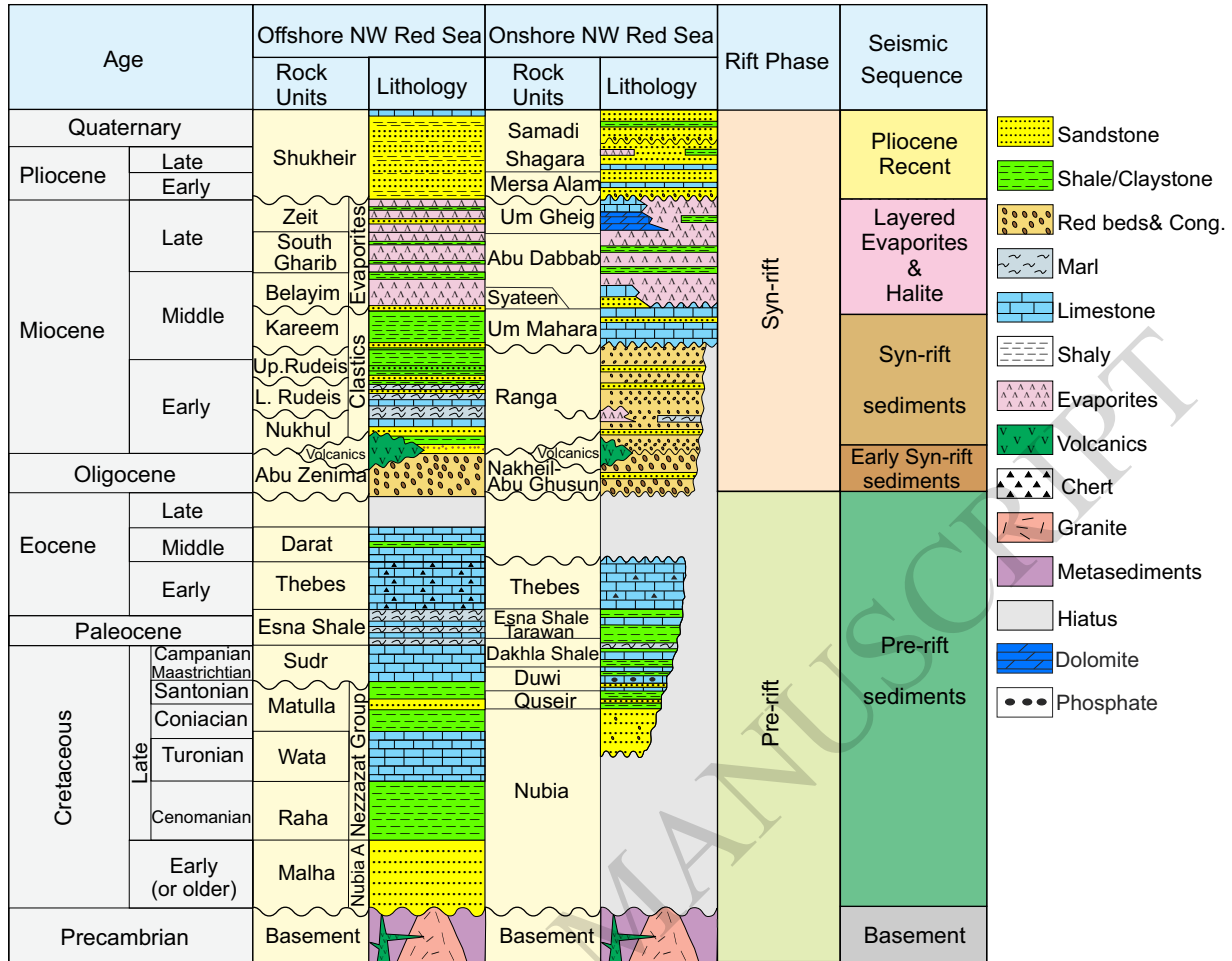


Figure 3



ACCEPTED MANUSCRIPT

Figure 4

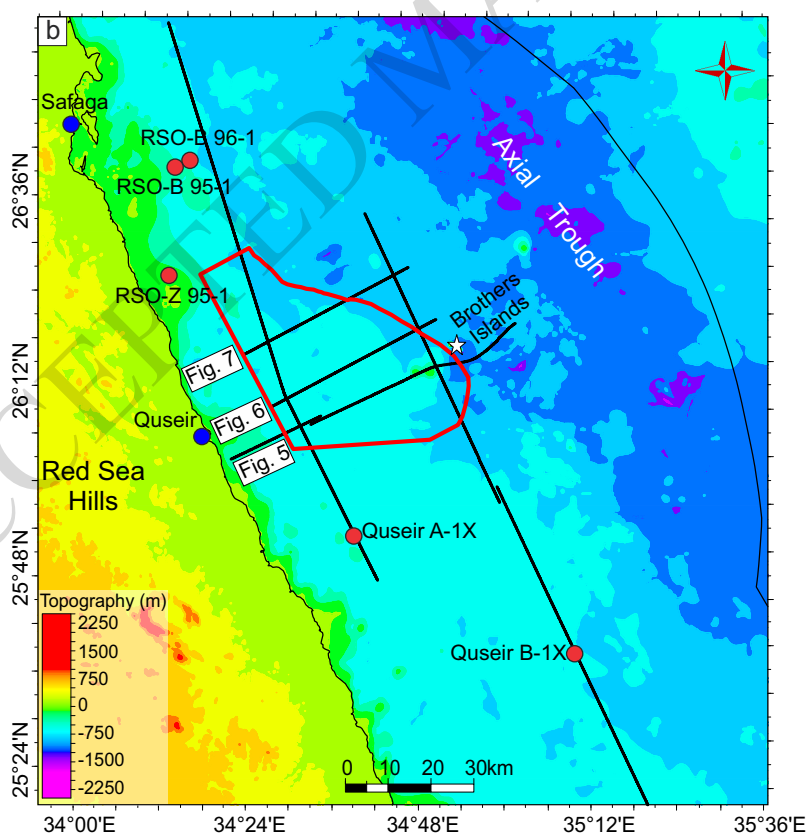
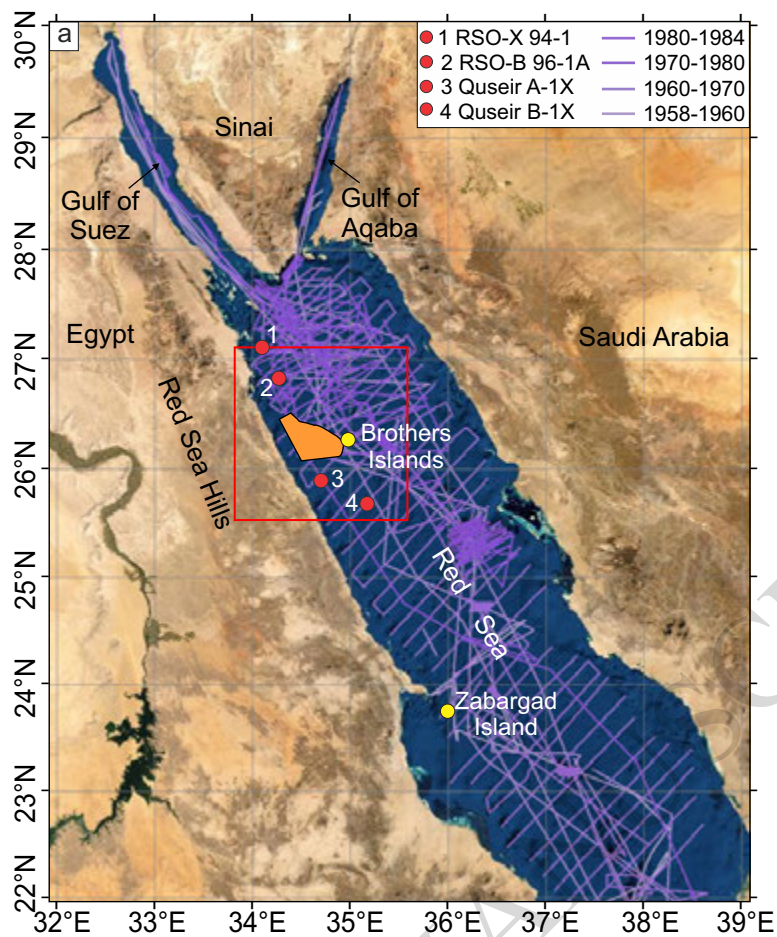


Figure 5

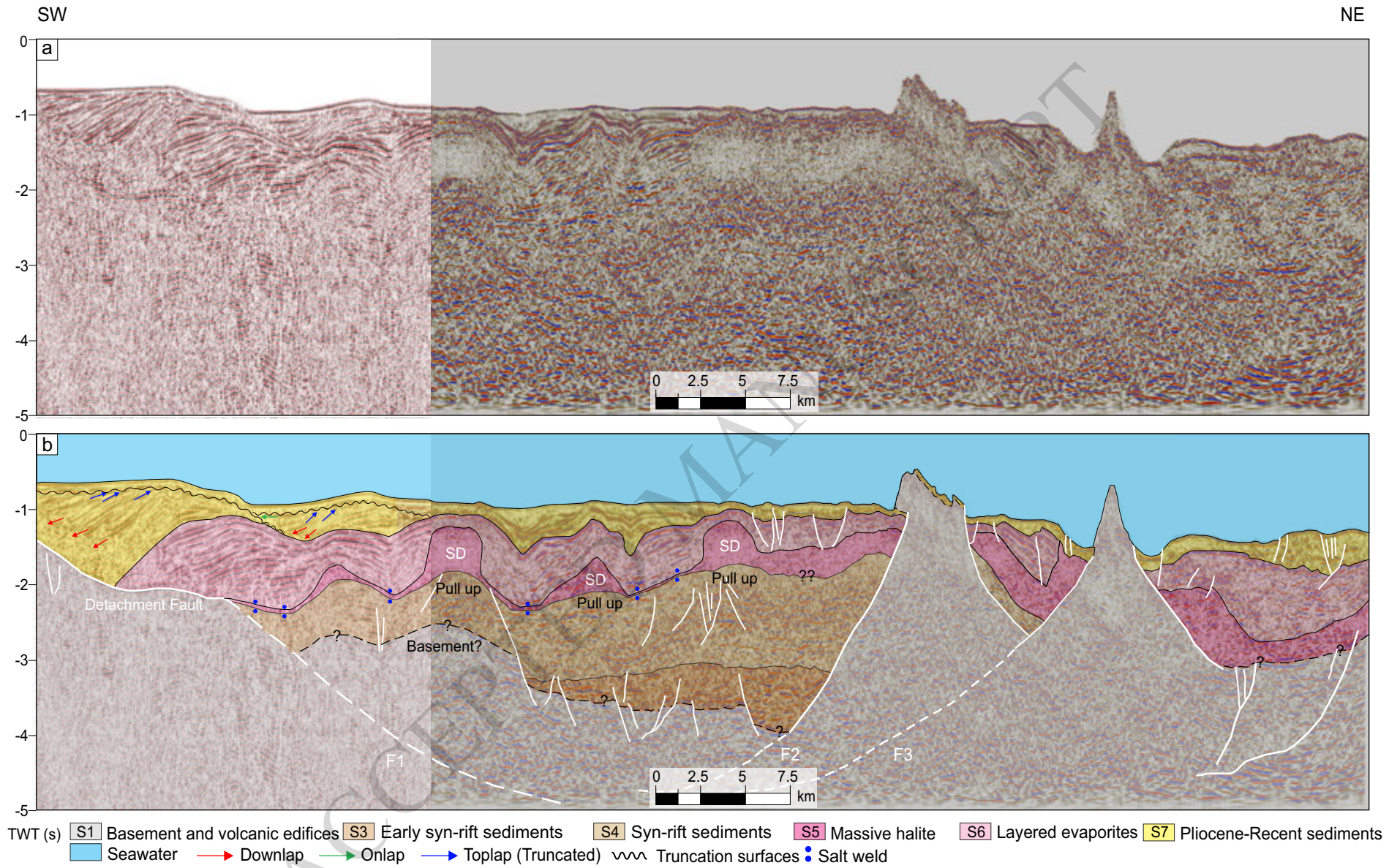


Figure 6

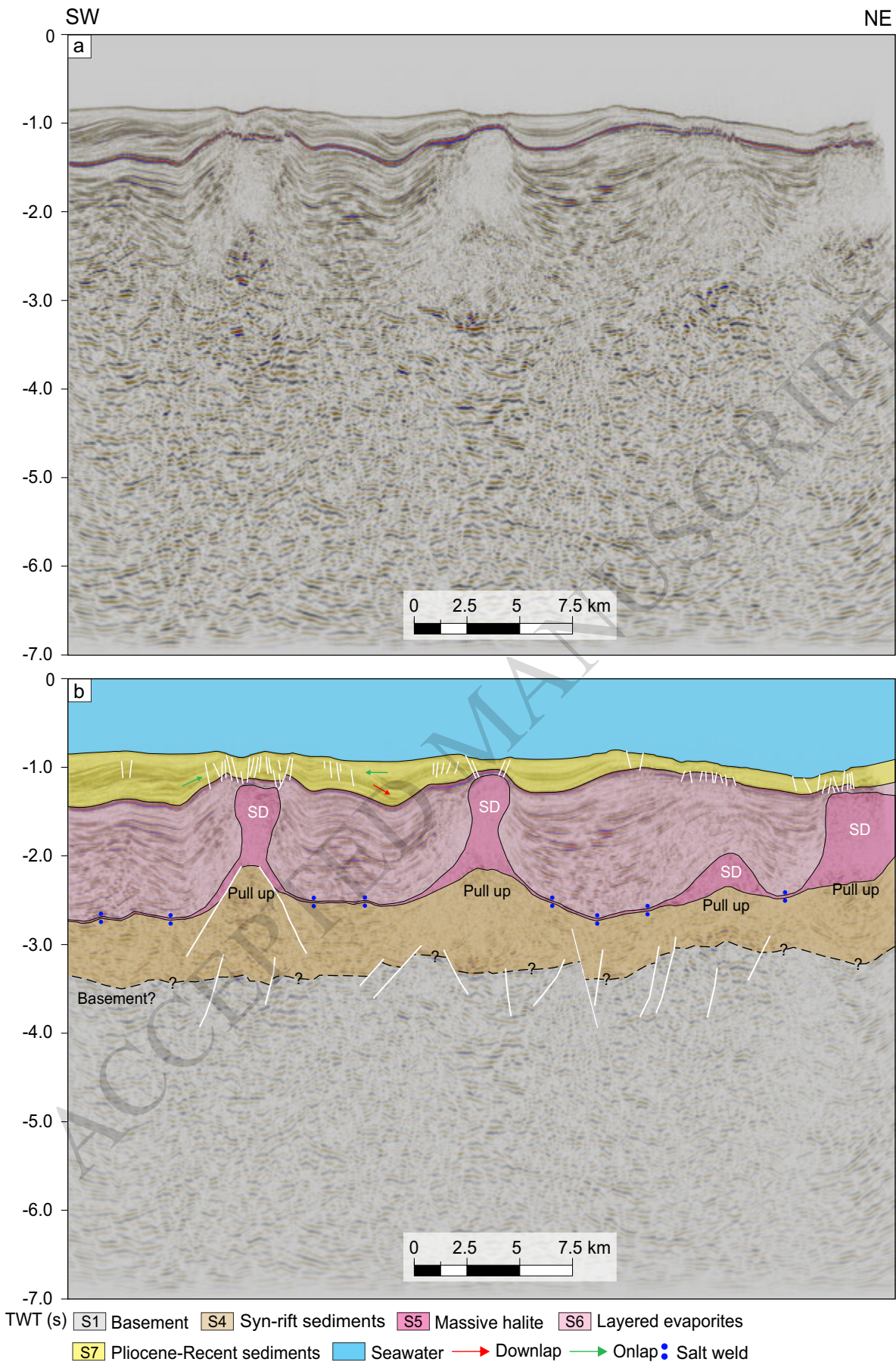


Figure 7

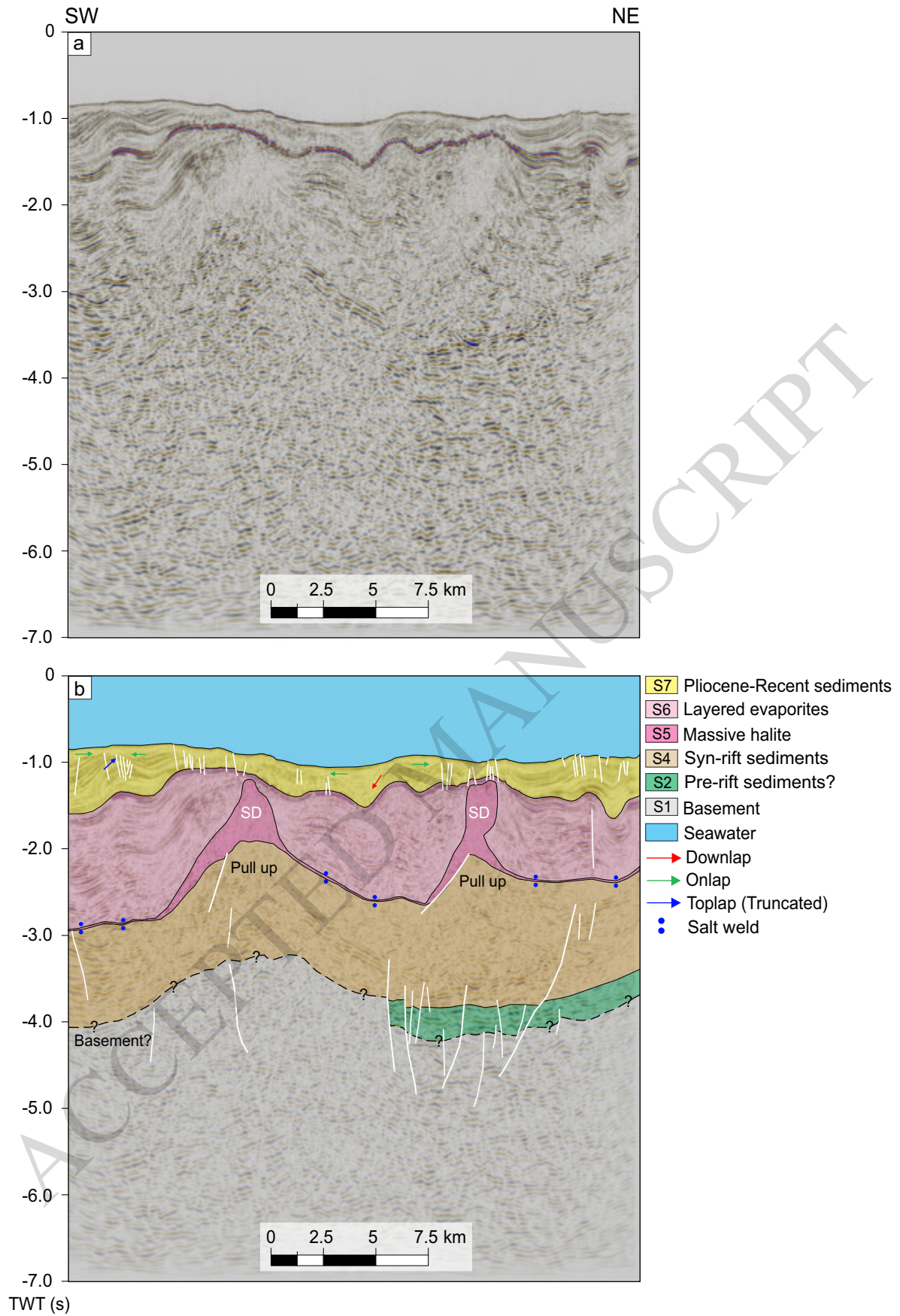
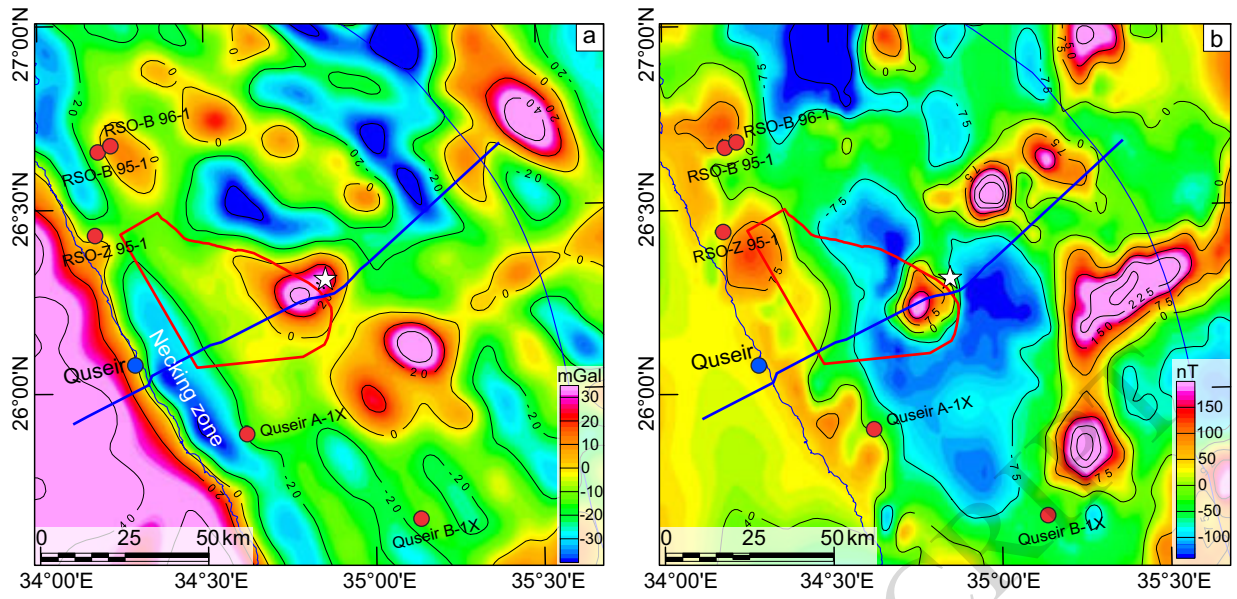


Figure 8



ACCEPTED MANUSCRIPT

Figure 9

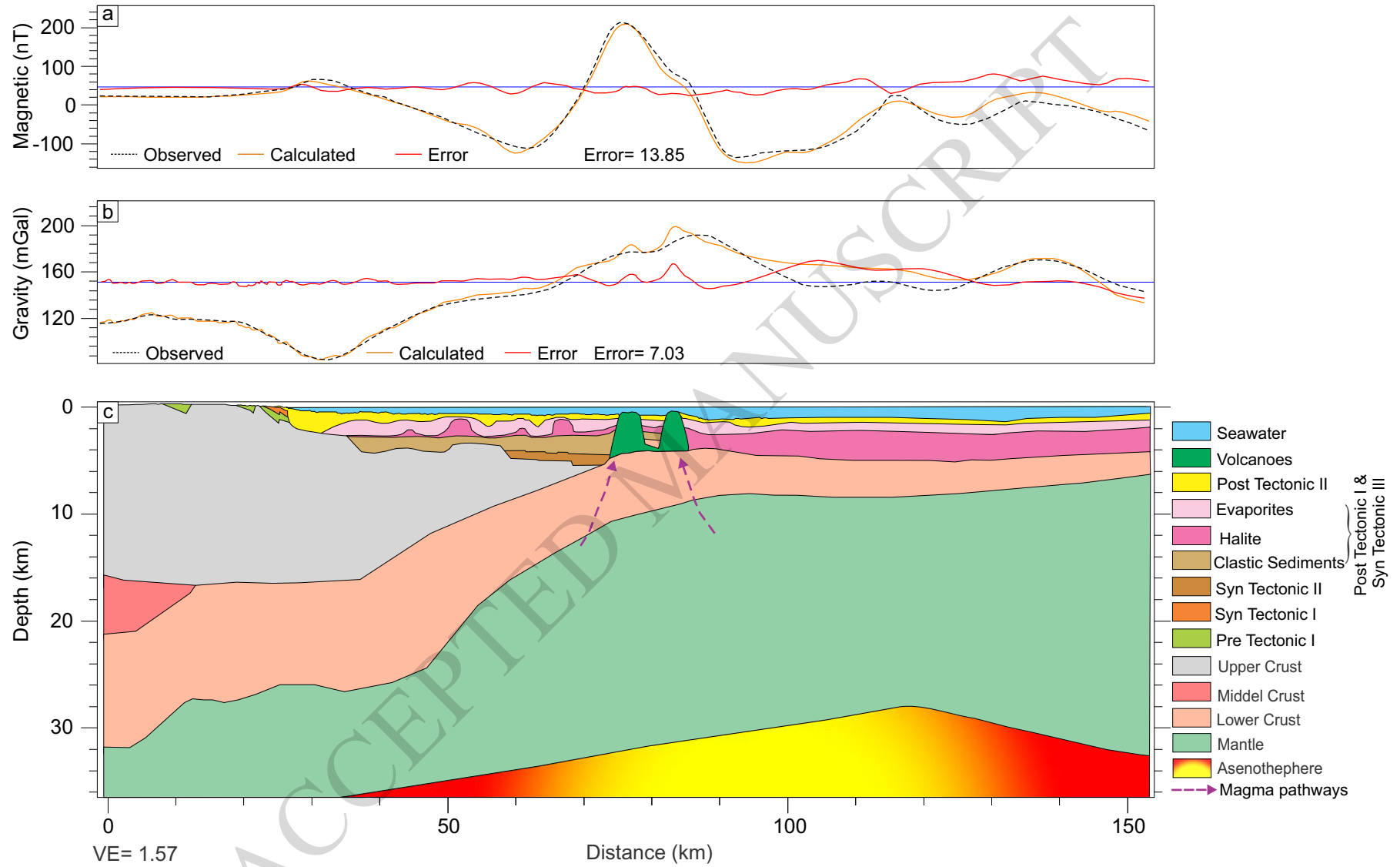


Figure 10

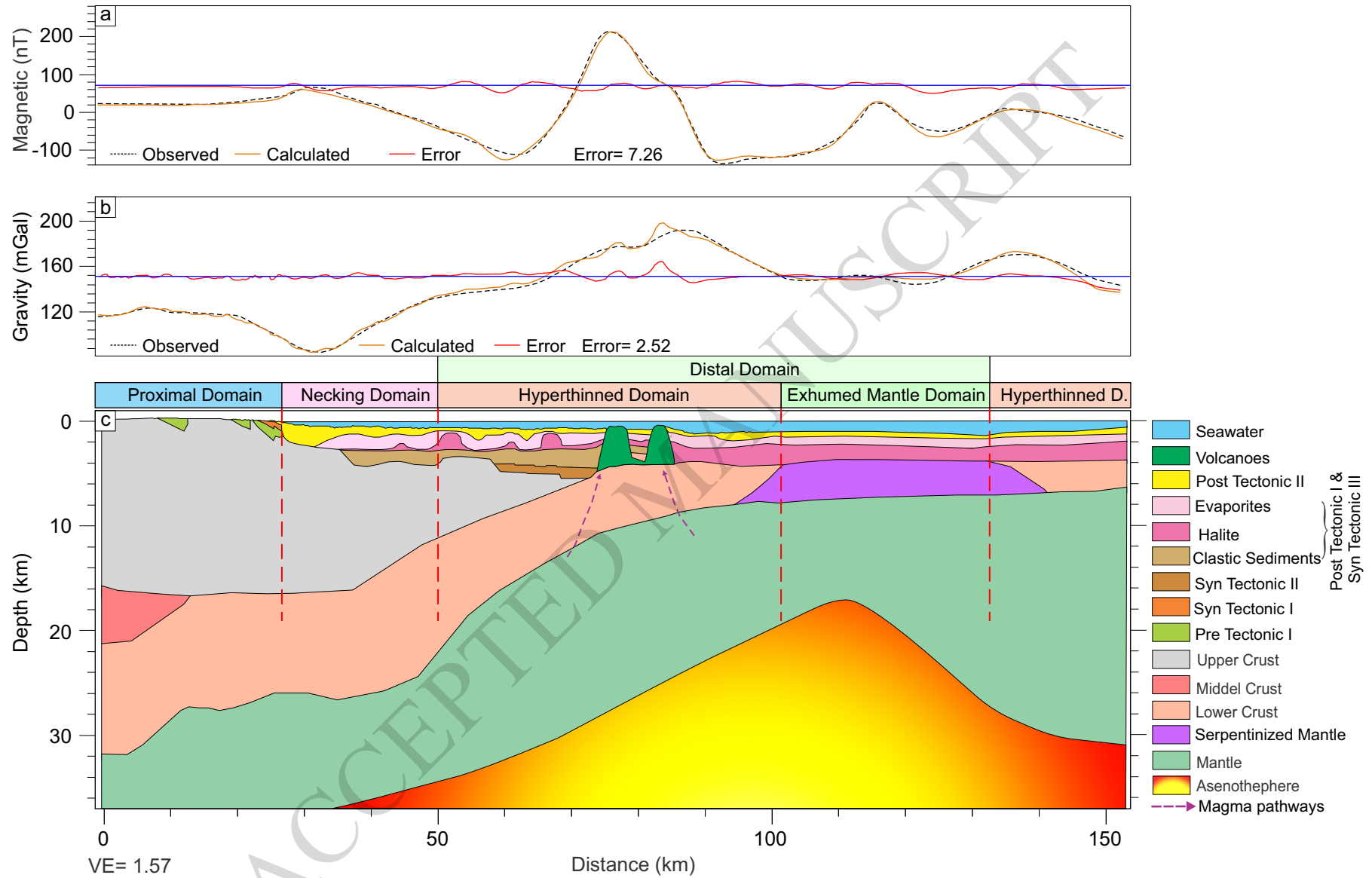


Figure 11

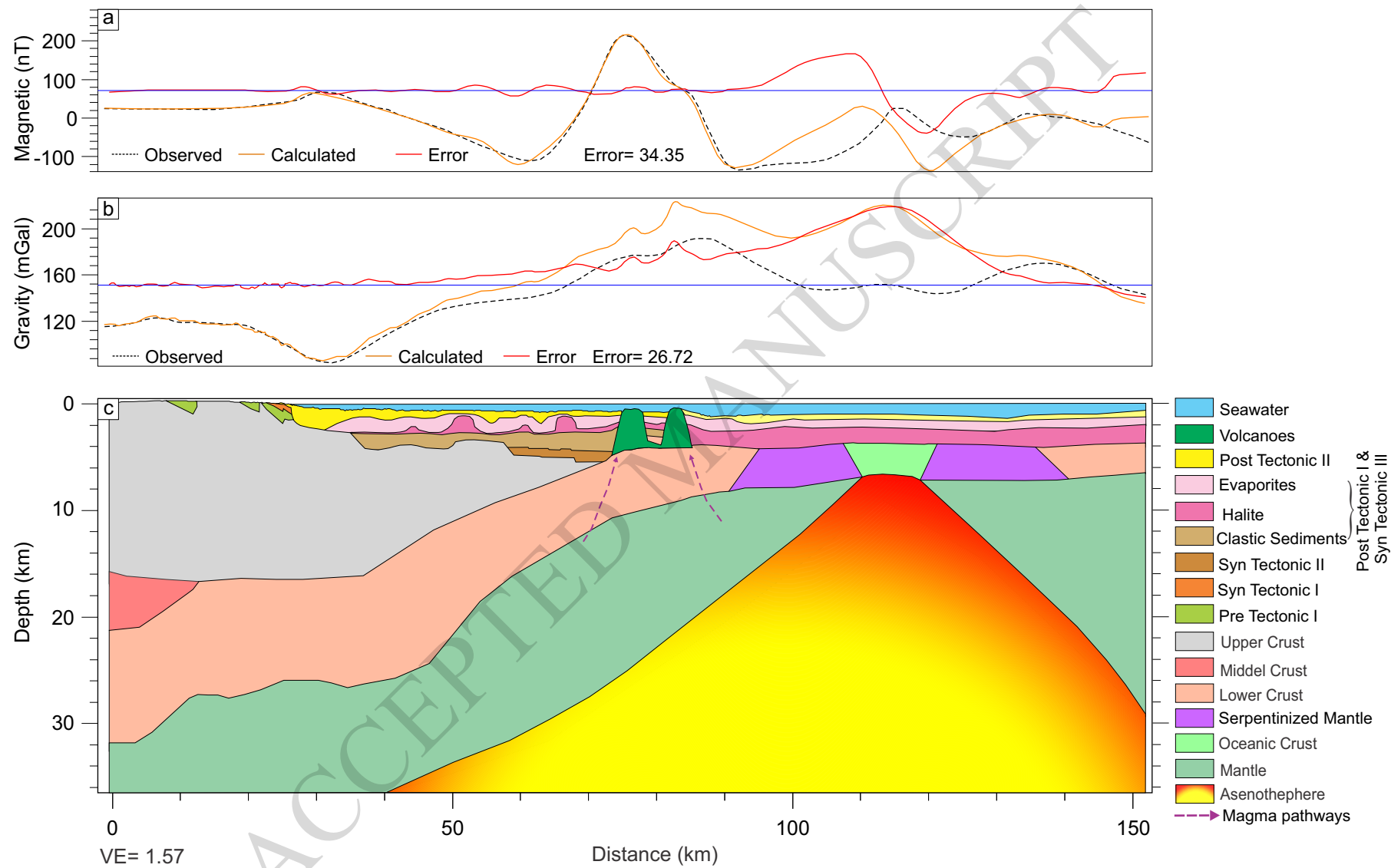


Figure 12a

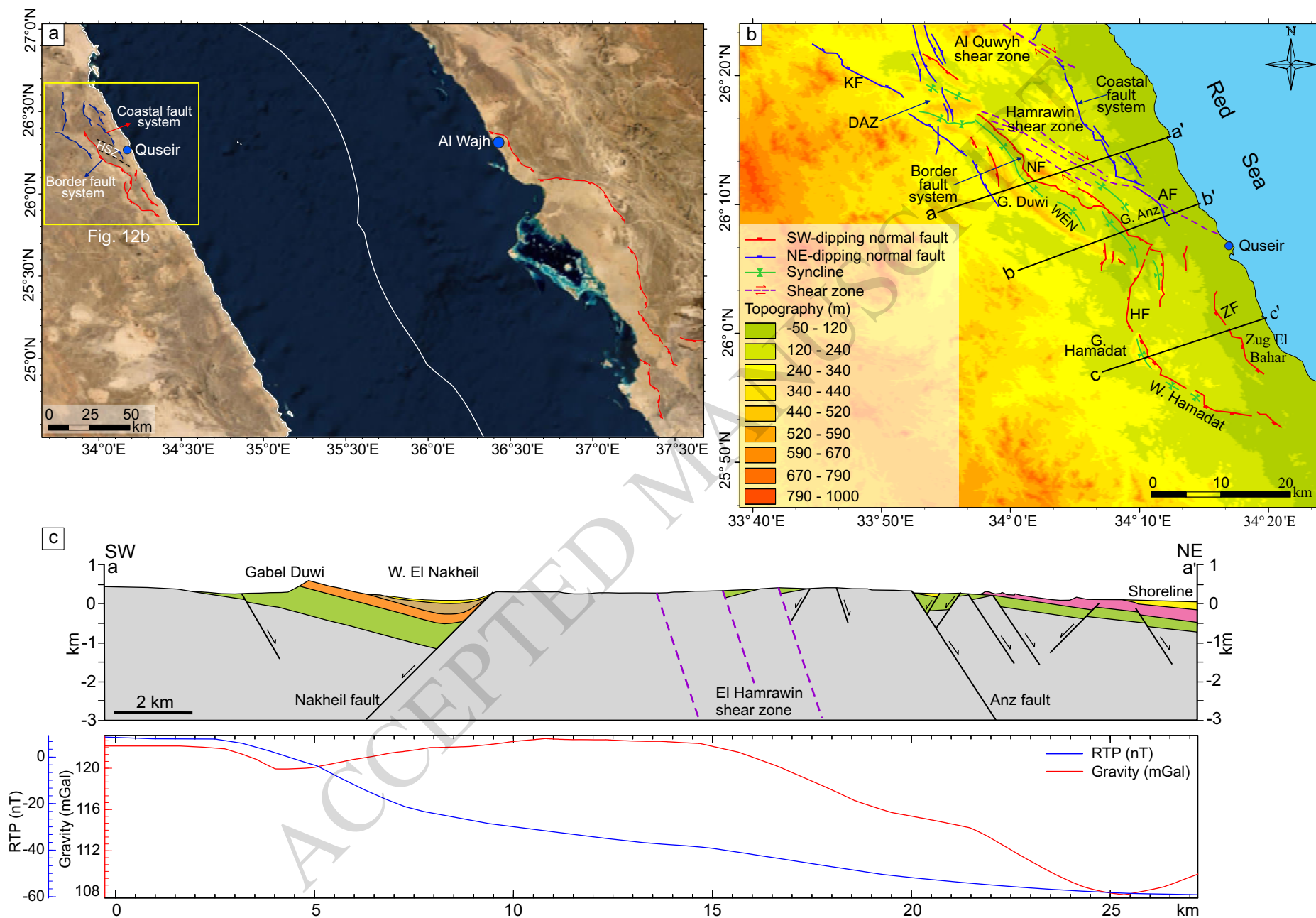


Figure 12b

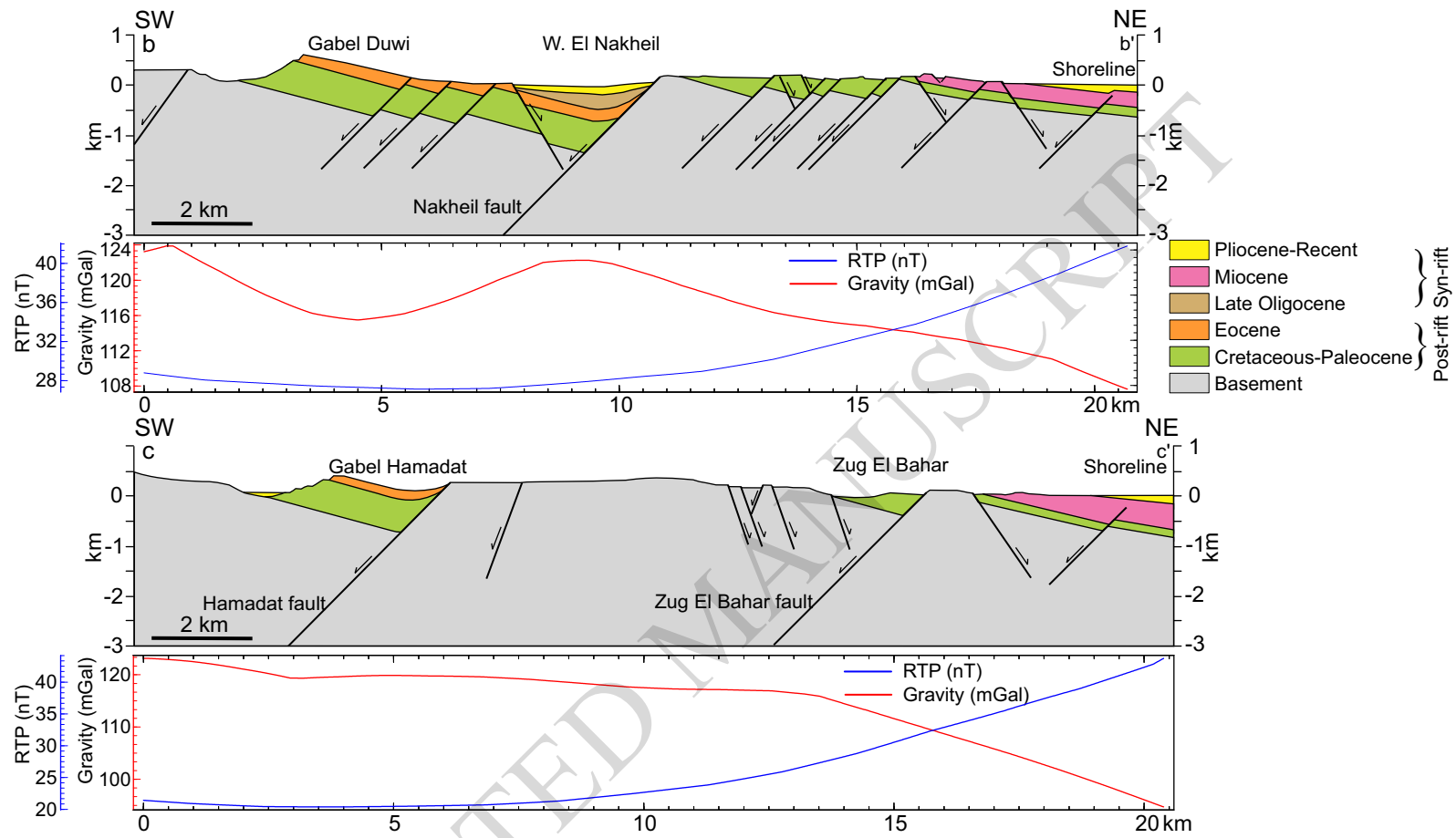
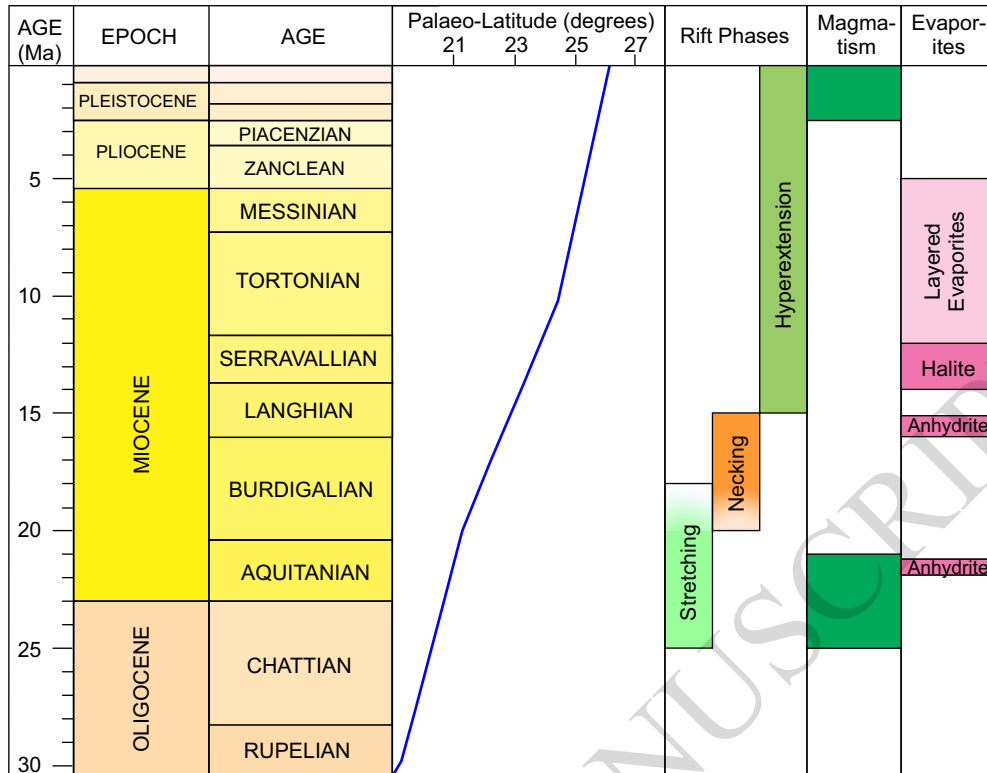




Figure 14



ACCEPTED MANUSCRIPT

Table 1

Unit Name	Average Density (g/cm <sup>3</sup> )	Average Susceptibility (u <sub>CGS</sub> )	Average Velocity (m/s)
Seamount	2.65	3400	3500
Pliocene-Recent sediments	2.2-2.35	0	1900
Layered evaporites	2.2-2.40	0	3300
Halite	2.1-2.25	0	4200
Syn-rift sediments	2.4-2.55	0-25	2700
Pre-rift sediments	2.3	0-50	2800
Upper Crust	2.68-2.8	450-1000	3500
Lower Crust	2.62-2.85	1200-6000	-----
Serpentinized Mantle	2.5-2.65	0	-----
Mantle	3.05-3.2	0	-----
Asthenosphere	3.1-3.25	0	-----

ACCEPTED MANUSCRIPT